



HAL
open science

Rates of carbon and oxygen isotope exchange between calcite and fluid at chemical equilibrium

Anna Harrison, Jacques Schott, Eric Oelkers, Katharine Maher, Vasileios Mavromatis

► **To cite this version:**

Anna Harrison, Jacques Schott, Eric Oelkers, Katharine Maher, Vasileios Mavromatis. Rates of carbon and oxygen isotope exchange between calcite and fluid at chemical equilibrium. *Geochimica et Cosmochimica Acta*, 2022, 335, pp.369-382. 10.1016/j.gca.2022.06.041 . hal-03811110

HAL Id: hal-03811110

<https://hal.science/hal-03811110>

Submitted on 11 Oct 2022

HAL is a multi-disciplinary open access archive for the deposit and dissemination of scientific research documents, whether they are published or not. The documents may come from teaching and research institutions in France or abroad, or from public or private research centers.

L'archive ouverte pluridisciplinaire **HAL**, est destinée au dépôt et à la diffusion de documents scientifiques de niveau recherche, publiés ou non, émanant des établissements d'enseignement et de recherche français ou étrangers, des laboratoires publics ou privés.

Rates of carbon and oxygen isotope exchange between calcite and fluid at chemical equilibrium

Anna L. Harrison^{a,b*}, Jacques Schott^a, Eric H. Oelkers^a, Katharine Maher^c, and Vasileios Mavromatis (Βασίλειος Μαυρομάτης)^a

^aGéosciences Environnement Toulouse (GET), Centre National de la Recherche Scientifique (CNRS), Observatoire Midi-Pyrénées, 14 Ave Edouard Belin, Toulouse, France 31400

^bSchool of Environmental Studies and Department of Geological Sciences and Geological Engineering, Queen's University, 36 Union Street, Kingston, Canada, K7L 3N6

^cDepartment of Earth System Science, Stanford University, Stanford, USA, 94305-2115

*corresponding author: anna.harrison@get.omp.eu

1 **Abstract**

2 The isotopic composition of carbonate minerals provides a record of historical
3 geochemical and environmental conditions, but the ability to interpret these compositions as
4 paleo-proxies hinges on their preservation over thousand to million year timescales. At chemical
5 equilibrium, alteration of initial isotopic compositions of calcite can occur in the presence of a
6 fluid without visible changes in morphology at the submicron scale, complicating the
7 interpretation of stable isotope compositions of carbonates. However, the rates and mechanisms
8 of isotope exchange at chemical equilibrium are poorly understood. To evaluate the rates and
9 processes by which C and O isotopes are exchanged between calcite and fluid, batch reactor
10 experiments were conducted at chemical equilibrium between calcite and a fluid enriched in ^{13}C
11 and ^{18}O relative to the solid at 25°C . Both natural and synthetic calcite of different grain sizes
12 were investigated to evaluate the impact of mineral surface area and size on C and O isotope
13 exchange rates. Our experimental results indicate that rapid exchange of both C and O isotopes
14 occurs within 72 h for all calcite grain sizes studied, likely indicative of exchange of surface
15 species in combination with a backward reaction during dissolution and Ostwald ripening of high
16 energy surface sites. After 72 h, C and O isotope exchange rates were slower but near constant
17 for timescales of thousands of hours. Surface-area normalized C and O isotope exchange rates
18 were similar for all calcite grain sizes studied, and O and C were exchanged in a $\sim 3:1$ ratio
19 consistent with exchange of CO_3^{2-} . The rates of C and O exchange were ~ 4 orders of magnitude
20 lower than far-from-equilibrium calcite dissolution rates, suggesting exchange was controlled
21 either by dissolution-precipitation of pre-existing reactive sites alone, or a combination of
22 dissolution-precipitation and solid state/aqueous mediated diffusion. Overall, the results of this
23 study suggest alteration of O and C isotope compositions of calcite at ambient temperatures can

24 proceed readily over short time scales, though the extent to which this process continues to
25 operate over geologic time scales is difficult to predict at present. The results of this study further
26 highlight the importance of generating a mechanistic understanding of the process of isotope
27 exchange at chemical equilibrium, and represent a step towards this understanding.

28

29 **Keywords:**

30 C isotopes, O isotopes, diffusion, dissolution-precipitation, isotopic alteration

31

32

33 **1. Introduction**

34 The isotopic composition of carbonate minerals provides a record of historical
35 geochemical and environmental conditions, generating a window into Earth's past. Calcium
36 carbonate minerals are abundant at Earth's surface and form by both biotic and abiogenic
37 processes, making them ideal archives of Earth's past environmental conditions. Trace metal,
38 major element, and isotopic compositions of carbonate minerals can be used to infer conditions
39 occurring at the time of mineral formation (Bernard et al., 2017; Coggon et al., 2010; Dekens et
40 al., 2002; Friedrich et al., 2012; Hoefs, 1997; Ravelo and Hillaire-Marcel, 2007; Urey et al.,
41 1951). Carbon, oxygen, and calcium isotopes in carbonates can be used to provide insights into
42 geochemical processes ranging from marine to groundwater environments including acting as
43 proxies for temperature, carbon cycle dynamics, and pH (Avrahamov et al., 2013; Bernard et al.,
44 2017; Fantle and Tipper, 2014; Friedrich et al., 2012; F"uger et al., 2019; Garnier, 1985; Gussone
45 et al., 2016; Hoefs, 1997; Katz et al., 2010; Marriott et al., 2004; Mavromatis et al., 2013, 2015,
46 2019; Mozeto et al., 1984; Ravelo and Hillaire-Marcel, 2007; Riechelmann et al., 2018; Spero et
47 al., 1997; Urey et al., 1951). To use any of these proxies effectively requires first that isotopic
48 and trace element compositions are preserved over timescales up to millions of years, and second
49 that the mechanisms of isotope fractionation are known. Samples that have undergone
50 recrystallization evidenced by observable morphological, chemical, or mineralogic features
51 detected by tools such as light or electron microscopy can be excluded from paleo-reconstruction
52 studies as the likelihood of poor preservation of isotopic compositions is obvious. For example,
53 calcitic foraminifera tests can be excluded from analysis when they appear "frosty" under light
54 microscopy due to recrystallization (Sexton et al., 2006). However, experimental studies have
55 revealed that isotopic compositions of calcite [CaCO₃] can be altered substantially without visual

56 evidence of recrystallization if isotopic disequilibrium between fluids and calcite occurs
57 (Bernard et al., 2017; Chanda et al., 2019; Cisneros-Lazaro et al., 2022; Géhin et al., 2021). The
58 mechanism and rate of this isotopic alteration will determine whether and under what conditions
59 carbonate archives preserve their isotopic compositions. Although a number of studies have
60 reported isotopic alteration of calcium carbonate and a variety of other minerals at chemical
61 equilibrium without morphological alteration observed at the scale of electron microscope
62 analysis, the mechanism of alteration of isotopic composition is yet to be fully understood (Beard
63 et al., 2010; Beard and Johnson, 2009; Curti et al., 2010; Frierdich et al., 2014; Géhin et al.,
64 2021; Gorski and Fantle, 2017; Oelkers et al., 2019).

65 There exist several mechanisms that can lead to alteration of isotopic compositions at
66 chemical equilibrium: exchange of surface species, solid state diffusion, and dissolution-
67 precipitation processes such as Ostwald ripening. In this study, these different processes are
68 defined as described below.

69 *Surface isotope exchange* involves the change in the isotopic ratio of the solid surface
70 sites (surface CO₃ groups in the present study) without bulk dissolution/precipitation impacting
71 deeper layers of the crystal. Exchange of surface species has often been invoked in isotope
72 exchange studies to explain the commonly observed initial rapid exchange of isotopes upon
73 interaction of isotopically different fluids and solids (Avrahamov et al., 2013; Géhin et al., 2021;
74 Mozeto et al., 1984; Stamm et al., 2019)

75 *Ostwald ripening* is a dissolution/precipitation process that occurs at (or near) bulk
76 chemical equilibrium to minimize the interfacial energy of a crystal or an ensemble of small
77 crystals. It drives the growth of the largest crystals at the expense of the smallest ones, and, for a
78 given crystal, the transfer of matter from the surfaces of excess surface free energy (affected by

79 defects, heterogeneities, etc.) to zones of lower surface free energy. Ostwald ripening has been
80 proposed as a mechanism for the exchange of isotopes between solutions and solids, especially
81 where diffusion in the solid is slow and crystals are small (Cole and Chakraborty, 2001; Dubnina
82 and Lakshatanov, 1997; Géhin et al., 2021).

83 *Dynamic equilibrium* is a dissolution/precipitation process that occurs at chemical
84 equilibrium and relates to the principle of detailed balancing, from which transition state theory
85 (TST) rate laws are constructed. In this process, it is assumed that the net reaction rate at
86 equilibrium is zero, yet continued transfer of mass may occur between solid and fluid with equal
87 forward (dissolution) and backward (precipitation) rates (Che et al. 2021, Oelkers et al., 2019;
88 Liu et al., 2016; Pearce et al., 2012; Mavromatis et al., 2015). Recent experimental studies have
89 utilized the principle of simultaneous forward and backward reactions (though not necessarily
90 TST) to estimate near-to-equilibrium reaction rates of a variety of minerals including calcite
91 (Subhas et al., 2017; Zhu et al., 2016), to account for equilibration of isotopic compositions
92 between fluid and solid after initial precipitation (Fernandez et al., 2019; Mavromatis et al.,
93 2016; Pearce et al., 2012) and to explain isotope exchange at or near chemical equilibrium
94 (Chanda et al., 2019; Grimm et al., 2021; Oelkers et al., 2019, 2018). However, the driving force
95 for dynamic equilibrium as a mechanism for isotope exchange is not clear, but could be related
96 to isotopic disequilibrium.

97 *Solid-phase diffusion* occurs within the crystal lattice by either interstitial or
98 substitutional mechanisms. In isotope diffusion (self-diffusion), controlled by substitutional
99 mechanisms, diffusion often depends on the availability of point vacancies throughout the crystal
100 lattice (Cole and Chakraborty, 2001). Solid-state diffusion has been invoked to explain both C
101 and O isotope alteration of biogenic calcite in the form of foraminifera tests in experiments at

102 90°C and above, and abiotic nano-crystalline calcite at 25°C (Bernard et al., 2017; Cisneros-
103 Lazaro et al., 2022; Géhin et al., 2021).

104 The term *stable mineral recrystallization* is defined by Gorski and Fantle (2017) as “a
105 reaction in which a stable mineral undergoes extensive exchange of atoms with ions in solution
106 with no overt changes in mineral structure, morphology or grain size.” Where “extensive” refers
107 to exchange of more than the atoms initially present at the solid-fluid interface (Gorski and
108 Fantle, 2017) and thus does not include solely surface isotope exchange. “Overt” refers to
109 changes not evident with macroscopic or microscopic tools, but is dependent on the observation
110 scale (Gorski and Fantle, 2017). In the present study, we consider changes observable at the scale
111 of electron microscopy to be overt. Stable mineral recrystallization does not explicitly define a
112 mechanism of exchange and could therefore include a combination of diffusion and dissolution-
113 precipitation processes that do not result in overt alteration of the mineral surface.

114 Identifying the mechanism of alteration of isotope composition in calcite is valuable, as
115 the mechanism will strongly influence both the overall extent of exchange and its time-
116 dependence. Diffusion and recrystallization could lead to significant alteration of isotopic
117 compositions and little preservation of the original mineral isotopic composition, whereas the
118 exchange of surface species would not have a substantial impact on bulk isotopic composition of
119 the mineral. Ostwald ripening is likely an important control on isotopic exchange in early stages
120 of mineral precipitation and growth for poorly crystalline materials and/or materials with surface
121 textures of excess surface energy. However, this mechanism is likely less important for well-
122 crystallized and aged materials. The objective of this study is to evaluate the rates of alteration of
123 C and O isotope compositions of calcite at 25°C and chemical equilibrium, and generate insights
124 into the possible mechanism. Chemical equilibrium is here defined as the equivalency of the ion

125 activity product of Ca and CO_3^{2-} and the solubility product of pure calcite. A series of batch
126 reactor experiments were conducted in which both natural and synthetic calcite of different grain
127 sizes were exposed to a fluid enriched in ^{18}O and ^{13}C relative to calcite at chemical calcite-fluid
128 equilibrium. This is the first study to our knowledge to evaluate O and C exchange
129 simultaneously, and at bulk calcite-fluid equilibrium with high purity calcite, allowing new
130 insights into the mechanisms and rates of isotope exchange.

131

132 **2. Methods**

133

134 *2.1. Experimental methods*

135

136 A series of batch reactor experiments was used to evaluate the rate of exchange of C and
137 O isotopes between calcite and co-existing fluid at chemical equilibrium and 25°C. A mass of
138 0.06 g of calcite was placed in each of 52 borosilicate glass vials in two experimental series.
139 Three different calcite grain sizes were used: a “large” and “small” grain size of a natural
140 Siberian spar, and a fine-grained synthetic calcite purchased from Merck. The natural calcite was
141 pulverized using an agate mortar and pestle and sieved to the desired grain size. The natural
142 calcite was rinsed and ultrasonically cleaned with ethanol after being sieved to remove fine
143 particulates. The first experimental series used only “large” natural calcite grains of 200-400 μm .
144 The second experimental series examined reproducibility of the large calcite results, by using
145 large natural calcite grains of 250-500 μm , and investigated the impacts of surface area on rates
146 of exchange using small natural calcite grains between 150-200 μm , and synthetic calcite (Table
147 1). Duplicate reactors of the large calcite were collected at a number of timepoints. The

148 properties of the initial calcite are described in Table 1. Three reactors contained solution only
149 with no calcite to serve as control experiments without fluid-solid interaction.

150 Experimental conditions of each series are summarized in Table 2. An initial solution that
151 was slightly undersaturated with respect to calcite was prepared for each of the two experimental
152 series (saturation index between -0.47 and -0.63). The initial solution was prepared using ^{18}O -
153 enriched water (97% ^{18}O) and ^{13}C -enriched NaHCO_3 (98% ^{13}C). The fluid for the first
154 experimental series was prepared using 23.84 g of the ^{18}O -enriched water diluted to 1159.09 g of
155 total fluid by mixing with non-enriched de-ionized water. A mass of 0.0671 g of ^{13}C -enriched
156 NaHCO_3 and 0.3245 g of non- ^{13}C -enriched NaHCO_3 was added to this fluid to obtain the desired
157 $\delta^{13}\text{C}$ and initial NaHCO_3 concentration. The initial solution for the second experimental series
158 was prepared by mixing 24.02 g of ^{18}O -enriched water diluted to 1024.49 g of total fluid by
159 mixing with non-enriched de-ionized water. A mass of 0.0672 g of ^{13}C -enriched NaHCO_3 with
160 0.3203 g of non- ^{13}C -enriched NaHCO_3 was added to this fluid. The calculated $\delta^{18}\text{O}$ and $\delta^{13}\text{C}$ of
161 the initial reactive solution for the first experimental series was 9861‰ VPDB (expressed as
162 VPDB for ease of comparison with solid compositions) and 18037‰ VPDB, respectively. The
163 calculated $\delta^{18}\text{O}$ and $\delta^{13}\text{C}$ of the initial reactive solution for the second experimental series was
164 9851‰ VPDB and 18301‰ VPDB, respectively. Although the initial isotopic composition of
165 the fluid could not be measured owing to the extreme values, the uncertainty based on weighing
166 error (balance repeatability) is less than 0.15% of the value. The initial solution composition was
167 adjusted to achieve close to equilibrium conditions with respect to calcite by adding $\text{CaCl}_2 \cdot 2\text{H}_2\text{O}$
168 to each initial reactive solution prior to putting it in contact with the calcite. The initial solutions
169 had concentrations of 4.0×10^{-3} M NaHCO_3 and 2.5×10^{-4} M CaCl_2 in the first experimental
170 series and 4.5×10^{-3} M NaHCO_3 and 2.8×10^{-4} M CaCl_2 in the second experimental series. The

171 initial saturation index of calcite in the solutions was -0.63 and -0.47 in the first and second
172 experimental series, respectively (calculated using PHREEQC as described below, with pH fixed
173 by charge balance). The borosilicate reactors were filled leaving no headspace using ~25 mL of
174 the initial solutions. The reactors were then sealed with screw tops, wrapped in parafilm, and
175 placed into a 25°C shaking water bath for the duration of each experiment.

176 Individual reactors were sampled in their entirety at selected times over 125 days for the
177 small and synthetic calcite and 592 and 219 days for the large calcite in the first and second
178 experimental series, respectively. Fluids were removed from each reactor using a 30 mL syringe
179 and filtered through a 0.22 µm polyethersulfone syringe filter. One aliquot was acidified to 2%
180 bi-distilled HNO₃ for subsequent analyses of Ca concentration and another aliquot remained
181 unacidified for pH and alkalinity measurement. Fluid pH was measured immediately following
182 sampling using a Metrohm 913 pH-meter and a Metrohm combined electrode (6.0234.1000) for
183 the first experimental series. The fluid pH was measured using a WTW pH 3310 portable meter
184 equipped with a SenTix 41 electrode for the second experimental series. The pH probes were
185 calibrated prior to each measurement period using pH 4.01, 7.00, and 9.18 (25 °C) buffer
186 solutions, with an uncertainty of approximately ±0.03 pH units. Care was taken to minimize
187 exposure to the atmosphere during sampling. The resulting solids from each reactor were
188 vacuum filtered onto a 0.45 µm filter. Solids were rinsed thoroughly with de-ionized water and
189 ethanol and dried at room temperature.

190

191 *2.2 Analytical methods*

192 *2.2.1 Fluid chemical composition*

193 Calcium concentration of the fluids collected from each experiment was analyzed by
194 atomic absorption spectroscopy (AAS) using a Perkin Elmer AAnalyst 400. Based on triplicate
195 analysis of samples, this method had an analytical error better than $\pm 2.55 \times 10^{-5}$ mol/L and
196 detection limit of 2.03×10^{-7} mol/L. Alkalinity was determined using an automated Schott
197 Titroline AlphaPlus titrator by HCl titration. Measurement uncertainty was determined by
198 repeated analysis of triplicate samples and an in-house NaHCO_3 standard and was better than
199 $\pm 9.54 \times 10^{-5}$ mol/L as HCO_3^- . Dissolved inorganic carbon (DIC) concentrations were calculated
200 using the measured fluid composition and PHREEQC V3 (Parkhurst and Appelo, 2013) with the
201 minteqv4 database. The uncertainty introduced by calculation of DIC from alkalinity is
202 unknown, therefore the same uncertainty as alkalinity measurements of $\pm 9.54 \times 10^{-5}$ mol/L was
203 applied to calculated DIC concentrations. Saturation indices of calcite and fluid speciation were
204 determined using the same PHREEQC V.3 calculations.

205

206 *2.2.2 Analysis of solids*

207 The initial synthetic and natural calcite used were analyzed by X-ray diffraction to
208 confirm the presence of calcite and identify trace phases, if present. A Bruker D8 Advance X-ray
209 diffractometer with Cu radiation was used. A scan speed of 76.8 s/step and $0.01^\circ/\text{step}$ was
210 utilized. The morphology of the initial calcite and select reacted samples was evaluated using an
211 FEI Quanta 650 field emission environmental scanning electron microscope (SEM) and a JEOL
212 JSM 7100F TTLS LV field emission SEM. The initial surface area of each initial calcite material
213 was determined using BET analysis with Kr gas with a Micromeritics Tristar II Plus (reported in
214 Table 1). The chemical composition of the initial calcite was measured by digesting the calcite in

215 bi-distilled HNO₃ and analyzing using inductively coupled plasma mass spectrometry (ICP-MS)
216 with a Thermoscientific iCap TQ (reported in Table 1).

217

218 2.2.3 Isotopic analyses

219 Carbon and oxygen isotope analyses of the initial and reacted calcite were conducted
220 with a GasBench II coupled to a ThermoFinnigan MAT 253 mass spectrometer at the Ruhr-
221 University Bochum in continuous-flow mode following the methodology of Breitenbach and
222 Bernasconi (2011). Solids were ground with an agate mortar and pestle and homogenized prior
223 to analysis. Between 90 and 120 µg of ground solid was weighed into borosilicate glass vials and
224 these samples were acid-digested at 70°C and analyzed together with international standards
225 NBS19, IAEA603, and CO-8. Results are reported as δ¹³C and δ¹⁸O solid with respect to the
226 Vienna PeeDee belemnite (VPDB) standard. The external standard deviation for oxygen and
227 carbon isotope ratios was ≤0.07 and ≤0.06 ‰, respectively (n = 17). The isotopic composition of
228 the fluids were not measured as the isotopic composition was too enriched relative to natural
229 values and calibration standards.

230 Delta notation is defined by equation (1):

231

$$232 \quad \delta^x A = \left(\frac{\left(\frac{x_A}{y_A} \right)_{sample}}{\left(\frac{x_A}{y_A} \right)_{standard}} - 1 \right) \times 1000 \quad (\text{Eq. 1})$$

233 where A refers to the element (C or O) and x and y refer to the mass of the heavier and
234 lighter isotope, respectively.

235

236 2.2.4 Isotope exchange rate calculations

237 The extent of isotope exchange was calculated as follows for carbon (eq. 2-4):

238
$$X_{^{13}\text{C}_{\text{calcite},t}} = (1 - F_{\text{calcite},i})X_{^{13}\text{C}_{\text{spike}}} + F_{\text{calcite},i}X_{^{13}\text{C}_{\text{calcite},i}} \quad (\text{Eq. 2})$$

239
$$F_{\text{calcite},i} + F_{\text{spike}} = 1 \quad (\text{Eq. 3})$$

240
$$C_m = F_{\text{spike}}m_{\text{C,calcite}} \quad (\text{Eq. 4})$$

241 where $X_{^{13}\text{C}_{\text{calcite},i}}$ and $X_{^{13}\text{C}_{\text{calcite},t}}$ are the mole fraction of ^{13}C in the calcite initially and at time t ,
242 $X_{^{13}\text{C}_{\text{spike}}}$ refers to the mole fraction of ^{13}C of the initial reactive fluid which is assumed not to
243 change substantially throughout the experiment, F_{spike} represents the fraction of C in the calcite
244 that originated from the initial reactive fluid, $m_{\text{C,calcite}}$ denotes the total moles of C in the initial
245 calcite, C_m refers to the total moles of C exchanged between calcite and fluid at the sampling
246 time, and $F_{\text{calcite},i}$ represents the fraction of C in the calcite that has not exchanged with the fluid
247 (i.e., maintains its original isotopic composition). The same approach is used for calculating the
248 fraction of oxygen exchanged between fluid and solid but considers the mole fraction of ^{18}O in
249 the solid and fluid. When applied to the bulk system (the total moles of C and O), this mass
250 balance approach is termed a “homogeneous model,” and it assumes that the exchanged solid has
251 the same isotopic composition as the initial fluid at all times (Gorski and Fantle, 2017). This
252 assumption is justified due to the very large enrichment of the fluid in both ^{18}O and ^{13}C , which
253 means that 1) the fluid isotopic composition can be treated as effectively constant and 2)
254 fractionation during exchange can be neglected. Using the homogeneous model, it is estimated
255 that the maximum change in the mole fraction of ^{13}C in solution would be 1.95% and the
256 maximum change in the mole fraction of ^{18}O in solution would be $\sim 4 \times 10^{-4}$ %. The use of the
257 homogeneous model to estimate the extent of C and O exchange is therefore justified.

258 The rate of C or O isotope exchange was calculated as follows (eq. 5):

259

260
$$rate = \frac{C_{m_t}}{t \cdot S \cdot M} \quad (eq. 5)$$

261

262 where C_{m_t} refers to the moles of C or O exchanged at time t as calculated using equations 2-4, t
263 is time of sampling of a given experiment (s), S refers to the specific surface area (m^2/g), and M
264 refers to the total mass of calcite in each reactor (g).

265

266 **3. Results**

267 *3.1 Calcite composition and morphology*

268

269 Both the initial synthetic and natural calcite did not contain any other phases detectable
270 by XRD (Figure 1). The trace metal composition and BET surface area of the initial natural and
271 synthetic calcite is reported in Table 1. The natural calcite had higher concentrations of most
272 measured trace elements compared to the synthetic calcite, with the exception of Sr, which was
273 present above the quantification limit in the synthetic but not natural calcite (Table 1). However,
274 in both cases, the initial calcite was of high chemical and mineralogical purity. The majority of
275 calcite surfaces imaged were not visibly altered in any of the experiments, nor were there
276 noticeable changes in calcite grain size before and after the experiment as observed using SEM
277 (Figure 2). The surfaces of the natural calcite remained rough, with small surface particles,
278 fractures, and sharp boundaries retained at the end of each experimental series (Supplementary
279 Information Figure S1a). At the surface of a low number of large calcite grains (~3 in one sample
280 only), small 2D rhombohedrons were observed consistent with minor precipitation, though it
281 could not be determined if these were truly new features post reaction or were initially present
282 but unobserved in the initial calcite (Supplementary Information Figure S1b). Synthetic calcite

283 grains remained smooth before and after the experiment at the scale of observation and no visible
284 alteration was observed (Figure 2).

285

286 *3.2 Temporal evolution of fluid composition*

287 The pH of the reactive fluid increased slightly during the first ~1056 h of the
288 experiments, from ~7.5 to ~8.0, consistent with minor dissolution of calcite to achieve
289 equilibrium (Figure 3). After this time, the reactive fluid pH remained relatively stable, between
290 7.97 and 8.20 in all experimental series. The pH of control experiments run in the absence of
291 calcite ranged between 7.83 and 7.97. The Ca concentration of the reactive fluid increased
292 rapidly during the first 72 h of each experimental series as calcite dissolved towards equilibrium,
293 after which it remained relatively stable throughout the experiments. The Ca concentration of the
294 reactive fluid after 72 h was an average ($n = 7$) of $3.71 \times 10^{-4} \pm 3.54 \times 10^{-5}$ M in the first large
295 calcite experimental series, and $3.53 \times 10^{-4} \pm 1.60 \times 10^{-5}$ M ($n = 14$) in the second experimental
296 series. The Ca concentration of the reactive fluid in the small natural calcite experimental series
297 was an average of $3.65 \times 10^{-4} \pm 1.60 \times 10^{-5}$ M after 72 h. The Ca concentration of the reactive
298 fluid was slightly lower in the experimental series containing synthetic calcite with an average
299 after 72 h of $3.35 \times 10^{-4} \pm 2.73 \times 10^{-5}$ M. The Ca concentration of the reactive fluid in the control
300 experiments conducted in the absence of calcite remained the same as initial concentrations
301 within error, indicating no measurable interaction between Ca in the fluid and the reactor walls,
302 and no significant calcite precipitation or evaporation. Dissolved inorganic carbon concentrations
303 remained relatively constant in all experiments between 4.0×10^{-3} and 5.1×10^{-3} M (Figure 3).

304 The initial solutions were slightly undersaturated with respect to calcite (saturation index
305 (SI) = -0.63 and -0.47). As Ca concentrations increased, the SI of calcite approached equilibrium
306 and remained effectively at equilibrium for the remainder of all experiments (Figure 3).

307

308 *3.3 Temporal evolution of calcite isotopic composition*

309

310 The initial $\delta^{13}\text{C}$ composition of the natural Siberian calcite spar used for the large and
311 small calcite experimental series was $-0.23 \pm 0.06\text{‰}$ ($n = 13$) and its initial $\delta^{18}\text{O}$ composition was
312 $-16.11 \pm 0.37\text{‰}$ ($n = 13$) (Table 3). The analysis of 13 different aliquots in total demonstrates only
313 minor heterogeneity in initial composition. The initial $\delta^{13}\text{C}$ and $\delta^{18}\text{O}$ composition of the synthetic
314 calcite was $-9.09 \pm 0.04\text{‰}$ ($n = 3$) and $-19.10 \pm 0.04\text{‰}$ ($n = 3$), respectively (Table 3). The $\delta^{13}\text{C}$ and
315 $\delta^{18}\text{O}$ compositions of the calcite in all experimental series increased over time although the
316 chemical composition of the fluid remained relatively constant (Figure 4). In all experiments, a
317 rapid increase in both $\delta^{13}\text{C}$ and $\delta^{18}\text{O}$ of calcite was observed by the first sampling point (either
318 44 or 72 h). This rapid increase was followed by a slower but consistent increase in $\delta^{13}\text{C}$ and
319 $\delta^{18}\text{O}$ of the solid throughout the remainder of the small and synthetic calcite experiments (Figure
320 4). In the large calcite experiments, the $\delta^{13}\text{C}$ and $\delta^{18}\text{O}$ composition of the calcite slowly
321 increased between 72 and ~2112 h, after which no clear trend in composition was observed, but
322 significant enrichment of the solids in ^{18}O and ^{13}C was sporadically recorded (Figure 4).

323 The extent of alteration of the $\delta^{13}\text{C}$ and $\delta^{18}\text{O}$ values of calcite was strongly dependent on
324 grain size. The change in calcite isotopic composition was greatest in the synthetic calcite
325 experiments, which had the finest grain size, followed by the small natural calcite, and the large
326 natural calcite. A similar change in calcite isotopic composition over time was observed for both

327 sets of large calcite experimental series, despite their slightly different grain sizes (200-400 μm
328 vs. 250-500 μm). In the large calcite experiments, $\delta^{13}\text{C}$ increased from $-0.23\pm 0.06\text{‰}$ to
329 $0.55\pm 0.06\text{‰}$ within 1679 h and $1.12\pm 0.06\text{‰}$ within 2112 h in the first and second experimental
330 series, respectively. The $\delta^{18}\text{O}$ values of the large calcite increased from $-16.11\pm 0.37\text{‰}$ to -
331 $15.81\pm 0.07\text{‰}$ within 1679 h and $-15.12\pm 0.07\text{‰}$ within 2112 h in the first and second
332 experimental series, respectively. In the small calcite experiments, $\delta^{13}\text{C}$ values of the calcite
333 increased from $-0.24\pm 0.06\text{‰}$ to $37.05\pm 0.06\text{‰}$ in 3000 h and $\delta^{18}\text{O}$ values of the calcite increased
334 from $-16.11\pm 0.37\text{‰}$ to $7.06\pm 0.07\text{‰}$. In the synthetic calcite experiments, $\delta^{13}\text{C}$ values of the
335 calcite increased to the greatest extent from $-9.09\pm 0.04\text{‰}$ to $48.30\pm 0.06\text{‰}$ in 3000 h, and $\delta^{18}\text{O}$
336 values of the calcite increased from $-19.10\pm 0.04\text{‰}$ to $16.49\pm 0.07\text{‰}$.

337 The small and synthetic calcite generally exhibited a continuous increase in $\delta^{13}\text{C}$ and
338 $\delta^{18}\text{O}$ values over time, albeit with some variability (Figure 4). The large calcite in both
339 experimental series exhibited a low but positive change in $\delta^{13}\text{C}$ and $\delta^{18}\text{O}$ values over time during
340 the first ~2112 h of the experiments (Figure 4). However, over longer time periods, large
341 variability in isotopic composition was observed in both large calcite experimental series. For
342 example, after 3000 h in the second large calcite series, the calcite in duplicate reactors had $\delta^{13}\text{C}$
343 values of $1.06\pm 0.06\text{‰}$ and $9.18\pm 0.06\text{‰}$ and $\delta^{18}\text{O}$ compositions of $-15.41\pm 0.07\text{‰}$ and -
344 $10.13\pm 0.06\text{‰}$. Similarly, in the first large calcite experimental series after 9437 h, the calcite in
345 duplicate reactors had $\delta^{13}\text{C}$ values of $4.73\pm 0.06\text{‰}$ and $0.61\pm 0.06\text{‰}$ and $\delta^{18}\text{O}$ compositions of -
346 $13.37\pm 0.07\text{‰}$ and $-15.56\pm 0.06\text{‰}$. Repeated analysis of different aliquots of large calcite samples
347 from the same reactor indicated the measurements were reproducible and likely not an artefact of
348 measurement error or substantial heterogeneity in initial or reacted calcite composition. For
349 example, the sample collected at 4656 h in the first large calcite experimental series was

350 measured three times, with a $\delta^{13}\text{C}$ composition of $26.69 \pm 1.06\text{‰}$ ($n = 3$) and $\delta^{18}\text{O}$ composition of
351 $-1.22 \pm 0.75\text{‰}$ ($n = 3$). The large enrichment in ^{13}C and ^{18}O in some large calcite reactors
352 exhibited no discernible trend though anomalously high $\delta^{13}\text{C}$ were generally coincident with
353 high $\delta^{18}\text{O}$ values. The lack of a temporal trend for the isotopic enrichment at longer timescales in
354 the large calcite experimental series is evidenced by the large differences between duplicate
355 reactors described, however it is noted that these sporadic high $\delta^{13}\text{C}$ and $\delta^{18}\text{O}$ values occurred in
356 both large calcite experimental series at times greater than ~ 3 months only and not in the small or
357 synthetic calcite experimental series.

358 The C and O exchange rate was calculated using equation 5, which indicated a similar
359 surface area normalized rate of exchange for both the small and synthetic calcite, and a
360 somewhat lower rate of exchange for the large calcite (Figure 5). Bulk rates, not normalized to
361 surface area, indicate the highest rate of exchange for the synthetic calcite, followed by the small
362 calcite, and finally the large calcite. After the initially rapid exchange during the first 72 h in all
363 experimental series, the C and O exchange rates were relatively constant throughout the
364 experimental series of the small and synthetic calcite and up to 2112 h in the large calcite
365 experimental series. Due to the highly variable $\delta^{13}\text{C}$ and $\delta^{18}\text{O}$ compositions of the large calcite
366 after 2112 h, only the data up to this time point are used to estimate exchange rates. The average
367 rate of C exchange after 72 h was $1.98 (\pm 0.57) \times 10^{-11}$ mol C/m²/s, $2.93 (\pm 0.83) \times 10^{-11}$ mol
368 C/m²/s, and $5.85 (\pm 1.42) \times 10^{-12}$ mol C/m²/s in the synthetic, small, and large calcite
369 experimental series, respectively. The average rate of O exchange after 72 h was $5.83 (\pm 1.65) \times$
370 10^{-11} mol O/m²/s, $8.69 (\pm 2.52) \times 10^{-11}$ mol O/m²/s, and $1.72 \pm (0.60) \times 10^{-11}$ mol O/m²/s in the
371 synthetic, small, and large calcite experimental series, respectively (Table 3). The average C and
372 O exchange rate of the large calcite experiments was determined using an average of both

373 experimental series between either 44 and 2112 h or 72 and 1678 h before the occurrence of
374 sporadic enrichment behaviour of ^{13}C and ^{18}O in both experimental series.

375 The molar ratio of O:C exchanged between calcite and fluid was an average of 2.93 ± 0.02 ,
376 2.97 ± 0.04 , 1.92 ± 0.56 , and 3.56 ± 0.64 in the synthetic, small, first large, and second large calcite
377 experimental series, respectively (Table 3, Figure 6). The O:C exchange ratio was relatively
378 constant in the synthetic and small calcite experimental series, increased over time in the first
379 large calcite experimental series, and decreased over time in the second large calcite
380 experimental series.

381

382

383 **4. Discussion**

384

385 *4.1 C and O exchange processes*

386

387 *4.1.1 Initial C and O isotope exchange*

388

389 In all experimental series, a rapid increase in $\delta^{13}\text{C}$ and $\delta^{18}\text{O}$ values was followed by a
390 lower, but fairly constant rate of increase for the remainder of the small and synthetic calcite
391 experimental series, and for up to ~ 2112 h in the large calcite experimental series. The change in
392 the O and C isotope exchange rates after 72 h may indicate a change in the isotope exchange
393 mechanism, or a change in reactivity of the solid over time or with depth as the reaction front
394 infiltrates further into the calcite particles. The initial rapid increase of the solid $\delta^{13}\text{C}$ and $\delta^{18}\text{O}$
395 values may be attributable to exchange of surface species (e.g., Avrahamov et al., 2013; Géhin et
396 al., 2021; Mozeto et al., 1984; Stamm et al., 2019). Assuming a density of calcite CO_3 surface
397 sites of 8.22×10^{-6} mol/m² (Pokrovsky et al., 2000), the complete exchange of surface sites
398 would result in 1×10^{-7} , 3×10^{-8} , 1×10^{-8} and 7×10^{-9} mols of C being transferred from the fluid to

399 the solid surface in the synthetic, small, first large and second large calcite experimental series,
400 respectively based on the BET surface area of each material. This would generate $\delta^{13}\text{C}_{\text{calcite}}$
401 values of -6.46, 0.48, -0.12, and -0.06 ‰, respectively. These values are significantly lower than
402 the measured $\delta^{13}\text{C}_{\text{calcite}}$ values (Table 3), which are consistent with up to 6.5-fold more C
403 exchanged than can be attributed to surface sites alone. Calculated $\delta^{18}\text{O}$ values are similarly
404 underestimated if exchange with the ideal surface site density is assumed. The implication is
405 either that the site density is greater than predicted or that the mineral-fluid interaction extended
406 beyond the surface layer. Calcite monolayers are ~0.5 nm thick (Subhas et al., 2017), indicating
407 approximately 7, 6, 3, and 2 surface layers of calcite would need to completely exchange with
408 the reactive fluid to produce the measured $\delta^{13}\text{C}$ values in the synthetic, small, and first and
409 second large calcite experimental series, respectively (assuming each layer is comprised of 8.22
410 $\times 10^{-6}$ mol CO_3/m^2). Similarly, approximately 6, 6, 1, and 2 surface layers of calcite would need
411 to completely exchange with the reactive fluid to produce the measured $\delta^{18}\text{O}$ values in the
412 synthetic, small, and first and second large calcite experiments, respectively. This extent of
413 exchange is consistent with previous observations of C exchange between calcite and seawater in
414 slightly undersaturated solutions, wherein 2 to 6 monolayers of calcite were observed to
415 exchange within 48 h of reaction as determined by Secondary Ion Mass Spectrometry (SIMS)
416 profiles (Subhas et al., 2017). In the present study, the fluids were initially slightly
417 undersaturated with respect to calcite and dissolved to reach equilibrium within ~72 h. Thus, a
418 similar process as documented by Subhas et al. (2017) may have operated in our experiments,
419 whereby a backward (precipitation) reaction during calcite dissolution at close-to-equilibrium
420 conditions results in isotopic alteration of the solid. In addition, Ostwald ripening involving the
421 dissolution of calcite surface domains of excess free energy followed by precipitation on surface

422 domains of lower free energy could have contributed to isotopic exchange during the initial
423 stages of the experiment, as these sites would exhibit greater reactivity than the bulk of the
424 calcite surface. In the present study, we estimate the extent of C and O exchange between fluid
425 and solid from the measured bulk isotopic compositions of the solids by mass balance. This
426 assumes that the exchanged solid has the same isotopic composition as the fluid. The use of this
427 approach may result in the underestimation of the number of monolayers impacted by isotopic
428 exchange. Nevertheless, the good agreement of the results of this study with those of Subhas et
429 al. (2017) suggests the observed rapid rate of exchange within the first 72 h of the experiment is
430 likely attributable to isotopic exchange between the first 2-6 monolayers of calcite and the fluid,
431 rather than a significant difference between the estimated and actual surface site density. The
432 interaction with 2-6 monolayers of calcite implies that the Ca and O isotope exchange may occur
433 by the combination of surface exchange, “backward” reaction, and Ostwald ripening (Géhin et
434 al., 2021; Subhas et al., 2017). The loss of some, but not all, fine particulates at the small calcite
435 surface over the course of the experiment is consistent with minor dissolution of the bulk crystals
436 over the first 72 h and Ostwald ripening of higher energy surface sites (Figure 2). Ostwald
437 ripening affecting approximately 0.3% of the surface of synthetic and small natural calcite grains
438 could account for the observed early C and O isotope exchange with a calcite dissolution rate
439 constant equal to $\sim 2 \times 10^{-7}$ mol/m²/s (Cubillas et al., 2005). In the case of large, well crystallized
440 natural calcite crystals, it seems likely that the contribution of Ostwald ripening to the early
441 isotope exchange should be less significant in accord with only approximately two surface layers
442 affected by complete exchange.

443

444 *4.1.2 Long-term C and O isotope exchange*

445

446 After the initial rapid exchange, the rate of C and O exchange between fluid and calcite
447 remained close to constant in the experimental series with small and synthetic calcite (Figure 5).
448 The C and O rates of exchange were also fairly constant between 72 and ~2112 h of the large
449 calcite experimental series before the sporadic behavior observed between ~ 2112 h and the end
450 of the ~14 208 h and 5256 h first and second large calcite experimental series, respectively
451 (Figure 5, Table 3). The extent of isotopic exchange during this slower exchange reaction using
452 the homogeneous model would result in an approximate depth of reaction of a further ~7, 20, 2,
453 and 1 nm, beyond that of the first 72 h in the synthetic, small, and first and second large calcite
454 experimental series, respectively. This approximate depth of interaction suggests surface
455 processes alone are not solely responsible for the continued isotopic alteration of the solid phase
456 over time. Here, we assess the potential contribution of solid state diffusion and dissolution-
457 precipitation processes to the continuous change in isotopic compositions of the solid phase.

458

459 4.1.2.1 *Evaluation of diffusive processes*

460

461 “Solid state” diffusion coefficients were estimated using the calculated moles of O or C
462 exchanged by mass balance (eq. 2-4) during the second, slower stage of solid isotopic
463 enrichment and equation 6 (Crank, 1975). As the extent of reaction is small compared to the
464 crystal size, the particle shape was neglected and diffusion equations relative to a semi-infinite
465 medium whose surface is maintained at a constant concentration were applied (Crank, 1975).
466 The assumption of constant concentration at the calcite surface is justified by the very large ¹⁸O

467 and ^{13}C enrichment of the spike relative to the solid. The following equation was used to
468 estimate the diffusion coefficients (eq. 6):

$$469 \quad \frac{M(t)}{a} = 2C_0 \left(\frac{Dt}{\pi} \right)^{0.5} \quad (\text{eq. 6})$$

470 where $M(t)$ is the moles of ^{18}O or ^{13}C transferred to the solid at a given time, D is the diffusion
471 coefficient (m^2/s), t designates time elapsed between the first sample and a later sample time (s),
472 a represents the total calcite surface area (m^2), and C_0 is the ^{13}C or ^{18}O concentration in the fluid
473 expressed as a mole fraction. D was calculated for the final time point in the synthetic and small
474 calcite experiments and at 1679 h and 2112 h in the first and second large calcite experiments,
475 respectively. The values of ^{13}C diffusion coefficients derived from Equation 6 for the long-term
476 exchange in all experiments are 1.3×10^{-24} , 1.1×10^{-23} , 4.2×10^{-26} , and 1.2×10^{-25} m^2/s in the
477 synthetic, small, and first and second large calcite experiments, respectively. The corresponding
478 values derived for ^{18}O diffusion coefficients are 1.3×10^{-24} , 1.0×10^{-23} , 2.0×10^{-26} , and 1.1×10^{-25}
479 m^2/s in the synthetic, small, and first and second large calcite experiments, respectively. These
480 diffusion coefficients are subject to substantial uncertainty as they are based on mass balance
481 calculations only. Thus, the reported diffusion coefficients should be considered order-of-
482 magnitude estimates at best.

483 The values of C and O isotope diffusion coefficients determined in the present study are
484 comparable to the values reported in literature for ambient temperature experiments that
485 investigated isotopic diffusion in calcite. Lahav and Bolt (1964) reported a diffusion coefficient
486 of Ca in calcite of 8×10^{-24} m^2/s , and Géhin et al. (2021) reported an effective diffusion
487 coefficient for C in calcite on the order of 10^{-25} m^2/s , both in experiments conducted at 25°C .
488 Notably, these experiments were conducted in the presence of a fluid phase, and the observed
489 isotope exchange may be influenced by dissolution-precipitation, or aqueous diffusion in water-

490 filled pores in addition to true solid-state diffusion (Anderson, 1969; Géhin et al., 2021).
491 Interestingly, Géhin et al. (2021) report that calcite stored in dry conditions did not show
492 evidence of isotopic exchange over similar timescales of their C aqueous isotope exchange
493 experiments, implying that the presence of a fluid has a strong impact on the apparent diffusion
494 coefficient of C in calcite. Fractures and higher porosity near the calcite surface, as observed in
495 the natural calcite (Figure 2), would facilitate aqueous-mediated diffusion, which is many orders-
496 of-magnitude faster compared to solid state diffusion (e.g., the diffusion coefficient of aqueous
497 species at 25°C is $\sim 8.00 \times 10^{-10} \text{ m}^2/\text{s}$ (Mayer et al., 2002)).

498 Despite good agreement of the calculated diffusion coefficients in the present work with
499 those previously reported for experiments conducted at 25°C, the estimated diffusion coefficients
500 in the present study are many orders of magnitude higher than those determined by extrapolation
501 from experiments conducted at high temperature. The majority of reported solid state diffusion
502 coefficients for O and C in calcite are from studies conducted at temperatures of >200°C and
503 range from 3×10^{-32} and $2 \times 10^{-65} \text{ m}^2/\text{s}$ when extrapolated to 25°C using the Arrhenius equation
504 (Anderson, 1969; Bernard et al., 2017; Haul and Stein, 1955; Kronenberg et al., 1984).
505 Compared to solid-state diffusion in single crystals, grain boundary diffusion of O is described
506 by a diffusion coefficient that is ~20 orders of magnitude larger at 25°C (Farver and Yund,
507 1998), similar to those measured in low temperature studies. Similarly, the complex,
508 interconnected porosity in foraminifera tests facilitate greater diffusive exchange between ¹⁸O-
509 enriched fluid and the solid compared to abiotic single calcite crystals (Cisneros-Lazaro et al.,
510 2022). The lack of agreement between diffusion coefficients from experiments conducted at
511 25°C versus those at high temperatures for single crystals suggests that the higher diffusion
512 coefficients at low temperatures may be attributable to the presence of fractures and

513 microporosity in the calcite and aqueous-mediated diffusion, possibly with some contribution of
514 dissolution-precipitation, rather than a solid-state process alone.

515 In the present study, the calculated ratio of O:C exchange is relatively close to the
516 expected stoichiometry of exchange of CO_3^{2-} for most of the experiments (Figure 6). This O:C
517 ratio is consistent with a dissolution-precipitation process as the carbonate ion (CO_3^{2-}) would be
518 incorporated or lost from the calcite solid. The stoichiometry that would be generated by a
519 diffusive process would also be 3:1 if diffusion occurred as CO_3^{2-} ions. Generally, C and O
520 diffusion coefficients in calcite have been documented to be of similar order of magnitude,
521 particularly at low pressure (Cherniak, 2010). At 100 MPA, O diffusion could be double that of
522 C due to a change in diffusion mechanism, with diffusion of CO_3 occurring primarily at lower
523 pressure (Cherniak, 2010). The rate of O diffusion in calcite is however, more sensitive than the
524 rate of C diffusion to factors such as Mn content of the calcite, $p\text{CO}_2$, and $p\text{H}_2\text{O}$, suggesting
525 some divergence in behavior could occur between C and O (Anderson, 1969; Kronenberg et al.,
526 1984; Labotka et al., 2011). The measured stoichiometry in the present study is consistent with
527 diffusion of the carbonate ion, as may be expected for solid state diffusion under certain
528 conditions, or diffusion of aqueous DIC (CO_3^{2-} , HCO_3^-).

529 The relative agreement between the estimated diffusion coefficients of our study and
530 those determined at similar temperatures implies that diffusion cannot be excluded as a potential
531 mechanism of C and O isotope exchange in our experiments. However, the trend of ^{13}C and ^{18}O
532 enrichment of the solid phase over time is not consistent with a pure diffusive mechanism, which
533 would tend to produce a parabolic temporal trend as implied by Eq. 6 (Figure 7). This suggests
534 that solid state diffusion is unlikely to be the only mechanism responsible for the isotopic
535 changes measured in the solid, regardless of the value of the diffusion coefficient.

536

537 *4.1.2.2 Evaluation of dissolution-precipitation processes*

538

539 Carbon and O isotope exchange over the longer timescales could also be attributed in part
540 to a dissolution-precipitation process such as Ostwald ripening. Although Ostwald ripening
541 likely contributed to the initial rapid isotope exchange within the first 72 h of the experiment, it
542 is less clear whether it could account for the longer-term isotopic alteration of the solid phase.
543 Apart from a loss of some fine grains at the surface of the small calcite, and a small number of
544 instances of possibly newly formed calcite islands on select large calcite grains, no pervasive or
545 consistent change in size or morphology of the calcite grains was documented during the
546 experiments at the submicron-scale resolution of SEM (Figure 2; Figure S1). The surface
547 roughness of both the small and large natural calcite was maintained throughout the experiments,
548 as was the dominance of aggregates of $>10\ \mu\text{m}$ scale crystals in the synthetic calcite; indicating
549 only minor, if any, surface restructuring occurred (i.e., below the resolution of SEM or occurring
550 in few enough locations to not be observed). The lack of observable alteration of the surface and
551 size of the calcite crystals suggests that dissolution-precipitation did not occur extensively. In
552 addition, the C and O isotope exchange rate is ~ 4 orders of magnitude lower than the predicted
553 dissolution rate of calcite at a pH of ~ 8 (Cubillas et al., 2005; Figure 5). It is not unexpected that
554 dissolution-precipitation rates are lower near-to-chemical equilibrium due to differences in
555 reaction mechanisms, for example, etch pits are not readily formed near-to-equilibrium
556 (Arvidson and Luttge, 2010; Hellmann and Tisserand, 2006; Schott et al., 2012, 1989; Subhas et
557 al., 2017). For instance, Subhas et al. (2017) observed a ~ 4 order-of-magnitude decrease in
558 calcite dissolution rates in seawater as equilibrium was approached. It is therefore possible that

559 the low rate of C and O exchange relative to dissolution of calcite at far-from equilibrium
560 conditions reflects dissolution-precipitation reactions only occurring at pre-existing reactive
561 sites, such as defects, that results in a much lower surface area-normalized dissolution and
562 precipitation rate compared to far-from-equilibrium conditions. This is consistent with the lack
563 of observable alteration of surface morphology, as only a limited portion of the reactive surface
564 would participate in the reaction. Reaction occurring only at pre-existing reactive sites implies
565 that the isotope exchange front is likely not homogeneous, and that ^{18}O and ^{13}C enrichment may
566 be concentrated only near defects and step edges; a hypothesis that requires imaging of C and O
567 isotope distribution to confirm. If sufficient highly reactive sites were available, a constant rate
568 of exchange of O and C would be expected, consistent with the relatively linear trends observed
569 in our experiments. Such a process is consistent with a type of Ostwald ripening of reactive
570 surfaces, as dissolution-precipitation at a small number of sites may not result in observable
571 surface alteration.

572 The measured C and O exchange rates in all experiments in the present study are in good
573 agreement with those reported by Chanda et al. (2019) for Ca isotope exchange between natural
574 abiotic calcite and fluid at 25°C (Figure 5). The good agreement between the exchange rate of C
575 measured in this study and the Ca exchange rate for abiotic calcite measured by Chanda et al.
576 (2019) suggests Ca and CO_3^{2-} are exchanged at similar rates, and thus potentially by similar
577 mechanisms. A similar rate of Ca and C exchange is consistent with a dissolution-precipitation
578 mechanism controlling isotopic exchange, as stoichiometric calcite dissolution and precipitation
579 would result in the same molar rate of Ca and C transfer between calcite and fluid. Alternatively,
580 similar solid state Ca and C diffusion coefficients and similar isotopic gradients would also result
581 in similar exchange rates. In contrast, the rates measured in the present experiments were at least

582 two orders of magnitude higher than C exchange rates between natural abiotic calcite and fresh
583 groundwater at 25°C reported by Avrahamov et al. (2013) (Figure 5). The reason for this
584 discrepancy may be due to the use of natural waters in the experiments of Avrahamov et al.
585 (2013), rather than the synthetic NaHCO₃-CaCl₂ solution used in this study. Fluid composition,
586 such as salinity and Mg concentration, has been observed to impact C isotope exchange rates,
587 with C isotopic exchange occurring at a slower rate in saline water compared to low salinity
588 water (Avrahamov et al., 2013; Mozeto et al., 1984). Moreover, the calcite solid used in the
589 Avrahamov et al. (2013) study contained impurities such as quartz, dolomite, and clays, which
590 may have additionally impacted isotopic exchange.

591 The surface-area normalized isotopic exchange rates were consistent between
592 experiments with synthetic and natural calcite, and between different grain sizes, implying that
593 the observed absolute rates of C and O isotope exchange were mainly dependent on surface area.
594 The extent of isotopic exchange by both dissolution-precipitation and diffusion is expected to
595 depend on calcite surface area. However, the observation of similar surface-area-normalized
596 exchange rates between natural and synthetic calcite is inconsistent with previous studies that
597 have reported differences in isotope exchange rates due to chemical or crystallographic
598 differences between synthetic and natural calcite, and between abiotic and biogenic calcite
599 (Chanda et al., 2019; Cisneros-Lazaro et al., 2022; Kronenberg et al., 1984; Lahav and Bolt,
600 1964). A difference in Ca isotope exchange rates between biogenic versus abiotic calcite in the
601 study of Chanda et al. (2019) could be attributed to the higher amount of chemical impurities in
602 the biogenic calcite, facilitating greater dissolution and reprecipitation due to compositional
603 differences between solid and fluid. Cisneros-Lazaro et al. (2022) also observed a more rapid
604 alteration of $\delta^{18}\text{O}$ composition of biogenic calcite in foraminifera tests compared to abiotic

605 calcite, which the authors attributed to a diffusive process facilitated by connected porosity in the
606 complex microstructure of the foraminifera. In the present study, both the natural and synthetic
607 calcite contained only trace levels of metal impurities, which could explain their similar
608 behavior. Moreover, the differences in morphology between natural and synthetic abiotic calcite
609 are far less significant than between abiotic and biogenic calcite.

610 The relatively small mass of O and C estimated to have exchanged between fluid and
611 solid based on bulk isotopic changes in the solids means that minor amounts of net precipitation
612 cannot be absolutely excluded as an explanation of isotopic alteration. The number of moles of C
613 incorporated in the solid to generate observed isotope changes is too small to generate a
614 significant change in Ca concentration. Thus, the lack of change in Ca concentration in most
615 experiments does not necessarily exclude a small amount of net precipitation. However, the lack
616 of measurable change in DIC and relatively consistent fluid saturation state, coupled with the
617 initial approach to equilibrium via dissolution, and the constant temperature of the experiments
618 suggest there was unlikely a substantial driving force for precipitation to occur within the
619 experiments, particularly at a constant rate over the entire duration of the experimental series.
620 Thus, although it cannot be completely ruled out based on available data, net precipitation is
621 unlikely the main process leading to isotopic alteration of calcite in the majority of reactors. The
622 exception, however, may be the late time behavior of the large calcite experimental series.

623 The sporadic enrichment of the large calcite in both ^{18}O and ^{13}C over the longest
624 experimental timescales has not been reported in previous studies, and the mechanism for its
625 occurrence in the present study is unclear. Nevertheless, it is consistent with the isotope
626 exchange rate being controlled by localized highly reactive sites rather than a homogeneous
627 process, be it diffusion or dissolution-precipitation reactions at highly reactive sites. The

628 reproducibility of measurements on aliquots of samples from a single reactor, even over different
629 analytical runs, suggests the observed changes are unlikely due to analytical issues with enriched
630 samples. Similarly, the sporadic enrichment behavior was not observed in the small and synthetic
631 calcite experiments which exhibited greater overall amounts of isotope exchange. We postulate
632 that the continuous shaking of the reactors could have led to the generation of fractures in or
633 roughening of the larger calcite crystals over time as they collided with each other and the
634 reactor walls. This would facilitate greater access of the enriched fluid into the crystals as well as
635 generate more highly reactive sites; the small islands of possible precipitates observed
636 infrequently could be a result of this process (Figure S1). Thus, more rapid isotope exchange or
637 incorporation of the enriched fluid could occur. The impact of this process would primarily be
638 observed in the large calcite experiments partly because they were sampled over a longer time
639 frame than the synthetic and small calcite experiments, and because the smaller particles with
640 higher initial surface area would not be as significantly impacted by small changes in surface site
641 availability.

642

643

644 *4.1.3 Summary of proposed C and O isotope exchange processes at chemical equilibrium*

645

646 Based on the observations of the present study, the following processes are proposed to
647 explain the observed C and O isotope exchange operating over different time frames in our
648 experiments. The first ~72 h of reaction is characterized by rapid exchange of surface species in
649 combination with small amounts of precipitation during net dissolution within the first ~72 h,
650 and Ostwald-ripening affecting surface areas of excess free energy on the calcite surfaces.

651 Between 72 h and ~2112 h during the large calcite experiments, and between 72 h and the end of
652 the small and synthetic calcite experiments at 3000 h, the precise mechanism of isotope
653 exchange remains ambiguous. However, the rates, time-dependent behavior, and stoichiometry
654 of C and O exchange may reflect a combination of solid-state diffusion enhanced by aqueous
655 diffusion in fractures and pores and dissolution-reprecipitation at existing steps or defects. The
656 dissolution-precipitation process may represent a type of Ostwald ripening, whereby sites of
657 higher surface energy are recrystallized to lower energy configurations. Finally, between ~2112
658 h and the end of the large calcite experiments, increased roughening of the calcite surface due to
659 particle-particle and particle-wall collisions generates reactive sites that promote isotope
660 exchange. The generation of reactive surface appears to be highly heterogeneous and does not
661 occur for all calcite grains. The generation of surface area in the large calcite reactors is
662 attributed to the experimental design, and is unlikely to be important for natural samples in
663 quiescent sediments.

664
665

666 *4.2 Implications*

667
668

669 The use of the isotopic compositions of carbonate minerals as archives of past
670 environmental conditions requires that the isotopic compositions imparted at the time of mineral
671 formation are maintained for long time scales of hundreds of thousands to millions of years.
672 When post-depositional recrystallization generates obvious chemical or morphological changes
673 in carbonate archives, carbonate samples that have been visibly or chemically altered can be
674 excluded from analysis. However, when isotopic compositions are altered without changes in the
675 morphology or chemical composition of the carbonate at scales observable by typical tools such
as light or scanning electron microscopy, it may not be possible to exclude isotopically altered

676 samples from analysis. Thus, it is necessary to understand the mechanisms and rates by which
677 isotopic compositions of carbonate minerals may be altered to ensure samples can be selected
678 and their compositions interpreted appropriately. Based on experiments conducted at 300°C,
679 Bernard et al. (2017) suggested that diffusive processes operating over long timescales may alter
680 $\delta^{18}\text{O}$ values of foraminifera tests in sediment archives to such a significant extent that paleo-
681 ocean temperature calculations may be altered by up to 15°C. Biogenic calcite tends to be altered
682 more rapidly than abiotic calcite in experimental systems (Chanda et al., 2019; Cisneros-Lazaro
683 et al., 2022), suggesting the abiotic carbonates like those used in our experiments may be less
684 susceptible to post-depositional alteration. However, the present study demonstrates that distinct
685 isotopic exchange between calcite and fluid can nevertheless occur at 25°C within short
686 timescales of hours to months. Importantly, mass balance of C and O isotope exchange in our
687 experiments demonstrates that the depth of isotopic alteration extends beyond the surface layer
688 and is likely at least several nanometers below the calcite surface. If the exchange reaction
689 continued to proceed at the same rate, it would take approximately 160 years to impact an entire
690 crystal the size of the crystal edge of small calcite (~187 μm). However, it is possible that the
691 rates may slow over time as the reaction front progresses further into the crystal so the
692 extrapolation to longer timescales is likely to be overestimated, and it is unknown how the
693 degree of isotopic equilibrium might impact exchange rates, if at all. If more realistic isotopic
694 differences between solid and fluid are assumed compared to the experiments, substantial
695 alteration of calcite isotopic compositions would occur if the experimental rates remained
696 constant over time (Supporting Information Figure S2). For example, at the rate of O isotope
697 exchange measured in the experiments with small natural calcite, it would take ~160 years for
698 calcite with a surface area of 0.065 m^2/g (equivalent to the small calcite) to reach isotopic

699 equilibrium with a fluid (Supporting Information Figure S2). Using the oxygen isotope
700 fractionation factor of Daëron et al. (2019), assuming a fluid composition of 0.5‰ (VSMOW),
701 the calcite isotopic composition would change from its initial value of 14.3‰ (VSMOW) to
702 31.3‰ (VSMOW; Supporting Information Figure S2). Our experimental results imply that
703 significant alteration of the isotopic composition of carbonate minerals in sediments is possible
704 even under chemical equilibrium within decadal timescales. It should, however, be noted that
705 extensive alteration of the isotopic composition of calcite in natural systems would require
706 sustained isotopic disequilibrium between fluid and solid. In our experiments, the moles of C in
707 the solid and fluid were nearly equal. On the other hand, in a marine sediment, there is a far
708 greater mass of C in the solid than the fluid, suggesting that the fluid isotopic composition is
709 likely to be dictated by the composition of the solid post-deposition in the absence of substantial
710 fluid flow (Grimm et al., 2021). In the absence of fluid flow, however, the decomposition of
711 organic carbon, if present in the system, could maintain C isotope disequilibrium between calcite
712 and fluid. In the case of oxygen, there is approximately only twice the number of moles of O in
713 the solid than the fluid in a cubic meter of marine calcite sediment (40% porosity; Fantle and
714 DePaolo, 2007). This suggests the oxygen isotope composition of the solid may be more
715 sensitive to alteration than carbon isotopic compositions.

716

717 **5. Conclusions**

718

719 The results of this study suggest that the alteration of O and C isotope compositions of
720 calcite at Earth's surface temperatures can proceed readily over short time scales, though the
721 extent to which this process continues to operate over geologic time scales is difficult to predict

722 at present. Rapid initial exchange between solid and fluid upon isotopic disequilibrium is
723 attributed mainly to exchange of surface species. The process by which the observed slower rate
724 of alteration of C and O isotope composition in calcite occurs over the longer time frames in or
725 experiments remains uncertain. Carbon and O isotope alteration over longer time scales (>72 h)
726 may proceed through a combination of dissolution-reprecipitation and solid state/aqueous
727 mediated diffusion. The great utility of isotopic and trace element compositions of carbonates,
728 however, highlights the necessity of a mechanistic understanding of solid-fluid exchange to
729 allow robust interpretation of archives and sample selection. The present study represents a step
730 towards this understanding, and demonstrates that abiotic calcite can undergo distinct C and O
731 isotope exchange at low temperature over timescales of as little as weeks to months without
732 morphologically visible evidence of alteration of the mineral.

733

734

735 **Acknowledgements**

736 The authors declare no competing interests. This study was supported by an NSERC Discovery
737 grant (05324-2019), an NSERC Postdoctoral fellowship, an INSU Tellus Syster grant, and a
738 Queen's University Research Initiation grant to ALH. Meredith Watson is thanked for her
739 assistance in the laboratory. We thank the AE, Mariette Wolthers, Hao Yan, and an anonymous
740 reviewer for their constructive comments that helped improve this paper. We also appreciate the
741 lab assistance and advice from Cristina Alvarez-Castillo and Andrea Perez-Fernandez, and
742 helpful discussion with Martin Voigt, Christian Grimm, Franziska Stamm, and Giuseppe Saldi.
743 We appreciate the AAS and alkalinity titration assistance from Carole Causserand. The Raimond
744 Castaing MicroCharacterization centre, particularly Arnaud Proietti, are thanked for their

745 facilitation of SEM analyses, along with Agatha Dobosz at Queen's University. Sylvia
746 Reichelmann and Sebastian Breitenbach are thanked for conducting the C and O isotope
747 analysis, and Ludovic Menjot (CNRS) for conducting the XRD analysis. We appreciate the
748 donation of the calcite spar from Oleg Pokrovksy.

749

750

751

752

753

754

755

756

757

758

759

760

761

762

763

764

765

766

767

768

769

770 Table 1. Characterization of initial calcite

Type	Size (μm)	BET surface area (m^2/g)	Trace element composition ^a							
			Mn (ppm) (± 6.41)	Fe (ppm) (± 12.94)	Zn (ppm) (± 3.72)	Sr (ppm) (± 0.67)	Y (ppm) (± 0.03)	La (ppm) (± 0.03)	Ce (ppm) (± 0.04)	Pb (ppm) (± 0.07)
large natural series 1	200-400	0.013	293.95	34.09	169.91	bq ^b	2.62	1.42	1.86	1.28
large natural series 2	250-500	0.019	293.95	34.09	169.91	bq	2.62	1.42	1.86	1.28
small natural	125-250	0.065	293.95	34.09	169.91	bq	2.62	1.42	1.86	1.28
synthetic	~10	0.222	bq	bq	bq	98.95	bq	bq	bq	bq

771 ^aelements present at > 1 ppm based on analysis of triplicate samples of initial natural and initial
 772 synthetic calcite

773 ^bbelow quantification limit

774

775 Table 2. Initial experimental conditions

Experimental series	Calcite type	Initial fluid $\delta^{13}\text{C}$ (‰ VPDB)	Initial fluid $\delta^{18}\text{O}$ (‰ VPDB)	Initial calcite saturation index
1	large natural	18037	9861	-0.47
2	synthetic	18301	9851	-0.63
2	small natural	18301	9851	-0.63
2	large natural	18301	9851	-0.63

776

777

778 Table 3. Solid isotopic composition, fluid chemical composition, and isotopic exchange rates
 779 over time

Experiment	Sample time (h)	$\delta^{13}\text{C}_{\text{PDB}}$ [‰]	$\delta^{18}\text{O}_{\text{PDB}}$ [‰]	Ca ($\times 10^{-4}$ mol/L)	DIC ^a ($\times 10^{-3}$ mol/L)	pH	C exchanged (moles)	O exchanged (moles)	C exchange Rate (mol/m ² /s)	O exchange rate (mol/m ² /s)
large natural calcite 1	0	-0.23	-16.11	1.82	4.55	7.52				
	44	0.25	-15.96	2.68	4.73	7.60	1.9×10^{-8}	2.6×10^{-8}	1.5×10^{-10}	2.0×10^{-10}
	334	0.33	-15.91	4.02	4.75	7.98	2.6×10^{-8}	3.8×10^{-8}	2.4×10^{-11}	3.5×10^{-11}
	669	0.54	-15.76	3.67	4.84	7.97	3.1×10^{-8}	5.9×10^{-8}	1.6×10^{-11}	3.0×10^{-11}
	1031	0.41	-15.99	3.61	4.24	8.15	2.6×10^{-8}	2.0×10^{-8}	8.8×10^{-12}	6.7×10^{-12}
	1679	0.55	-15.81	3.52	4.05	8.09	3.2×10^{-8}	5.1×10^{-8}	6.5×10^{-12}	1.1×10^{-11}
	2399	1.12	-15.44	3.95	4.00	7.90	5.4×10^{-8}	1.1×10^{-7}	7.9×10^{-12}	1.6×10^{-11}
	3103	0.71	-15.61	4.10	4.29	7.73	3.8×10^{-8}	8.4×10^{-8}	4.2×10^{-12}	9.4×10^{-12}
	4657	26.69	-1.22	3.08	4.33	7.82	1.1×10^{-6}	2.5×10^{-6}	8.0×10^{-11}	1.9×10^{-10}
	7374	10.43	-10.12	3.37	4.42	7.98	4.2×10^{-7}	1.0×10^{-6}	2.0×10^{-11}	4.8×10^{-11}
	9438	4.73	-13.37	3.49	4.10	7.90	2.0×10^{-7}	4.6×10^{-7}	7.3×10^{-12}	1.7×10^{-11}
	9438_duplicate	0.61	-15.56	nd	nd	7.81	3.4×10^{-8}	9.4×10^{-8}	1.3×10^{-12}	3.4×10^{-12}
	10754	26.52	-0.89	2.98	3.98	7.80	1.1×10^{-6}	2.6×10^{-6}	3.5×10^{-11}	8.3×10^{-11}
	14208	25.21	-1.53	3.22	4.14	7.99	1.0×10^{-6}	2.5×10^{-6}	2.5×10^{-11}	6.0×10^{-11}
large natural calcite 2	0	-0.23	-16.11	2.69	4.56	8.32				
	72	0.21	-15.72	3.74	4.91	7.75	1.8×10^{-8}	7.6×10^{-8}	5.8×10^{-11}	2.4×10^{-10}
	432	0.33	-15.63	3.67	5.02	7.83	2.3×10^{-8}	9.2×10^{-8}	1.2×10^{-11}	4.9×10^{-11}
	744	0.33	-15.62	3.54	4.99	7.87	2.3×10^{-8}	9.3×10^{-8}	7.2×10^{-12}	2.9×10^{-11}
	1056	0.26	-15.57	3.84	4.86	7.94	2.0×10^{-8}	1.0×10^{-7}	4.5×10^{-12}	2.3×10^{-11}
	1056_duplicate	0.41	-15.56	3.61	4.69	8.05	2.7×10^{-8}	1.1×10^{-7}	5.7×10^{-12}	2.3×10^{-11}
	1440	0.64	-15.45	3.78	4.94	8.04	3.8×10^{-8}	1.4×10^{-7}	5.7×10^{-12}	2.0×10^{-11}
	1752	0.52	-15.52	3.46	4.25	8.06	3.0×10^{-8}	1.1×10^{-7}	4.0×10^{-12}	1.5×10^{-11}
	2112	1.12	-15.12	3.50	nd	8.16	5.8×10^{-8}	2.0×10^{-7}	6.1×10^{-12}	2.1×10^{-11}
	2112	0.99	-15.26	3.48	4.33	8.11	5.4×10^{-8}	1.8×10^{-7}	5.5×10^{-12}	1.8×10^{-11}
	2448	3.08	-13.93	3.51	4.37	8.20	1.4×10^{-7}	4.3×10^{-7}	1.3×10^{-11}	4.0×10^{-11}
	2784	4.68	-12.87	3.38	4.38	8.14	2.1×10^{-7}	6.4×10^{-7}	1.7×10^{-11}	5.2×10^{-11}
	3000	9.18	-10.13	3.51	4.34	8.12	3.9×10^{-7}	1.2×10^{-6}	3.0×10^{-11}	8.9×10^{-11}
	3000_duplicate	1.06	-15.41	3.42	4.44	8.11	5.2×10^{-8}	1.3×10^{-7}	4.1×10^{-12}	1.0×10^{-11}
5256	14.19	-6.92	3.21	4.33	8.00	6.4×10^{-7}	1.9×10^{-6}	2.6×10^{-11}	7.8×10^{-11}	
5256_duplicate	3.72	-13.47	3.49	4.32	8.06	1.6×10^{-7}	5.1×10^{-7}	7.1×10^{-12}	2.2×10^{-11}	
Average ^b								$5.85 \pm 1.43 \times 10^{-12}$	$1.72 \pm 0.60 \times 10^{-11}$	
small natural calcite	0	-0.23	-16.11	2.69	4.56	8.32				
	72	5.09	-12.73	3.74	4.97	7.82	2.1×10^{-7}	6.3×10^{-7}	2.1×10^{-10}	6.2×10^{-10}
	432	6.26	-11.92	3.81	4.80	7.93	2.6×10^{-7}	8.1×10^{-7}	4.2×10^{-11}	1.3×10^{-10}
	744	8.48	-10.68	3.59	5.10	7.95	3.4×10^{-7}	1.0×10^{-6}	3.3×10^{-11}	9.6×10^{-11}
	1056	6.10	-12.16	3.82	5.05	7.30	2.5×10^{-7}	7.4×10^{-7}	1.7×10^{-11}	4.9×10^{-11}
	1440	14.55	-6.97	3.64	4.71	8.05	5.9×10^{-7}	1.7×10^{-6}	2.9×10^{-11}	8.4×10^{-11}
	1752	23.51	-1.43	3.37	4.11	8.10	9.5×10^{-7}	2.8×10^{-6}	3.8×10^{-11}	1.1×10^{-10}
	2112	20.88	-2.91	3.64	4.79	8.14	8.6×10^{-7}	2.5×10^{-6}	2.8×10^{-11}	8.3×10^{-11}
	2448	19.16	-3.86	3.50	4.78	8.06	8.0×10^{-7}	2.4×10^{-6}	2.2×10^{-11}	6.6×10^{-11}
	2784	20.54	-2.94	3.47	4.60	8.03	8.6×10^{-7}	2.6×10^{-6}	2.1×10^{-11}	6.2×10^{-11}
3000	37.05	7.06	3.14	4.74	8.08	1.5×10^{-6}	4.4×10^{-6}	3.5×10^{-11}	1.0×10^{-10}	
Average ^b								$2.93 \pm 0.83 \times 10^{-11}$	$8.69 \pm 2.52 \times 10^{-11}$	
synthetic calcite	0	-9.09	-19.10	2.69	4.56	8.32				
	72	8.78	-8.17	3.67	4.63	7.87	7.5×10^{-7}	2.2×10^{-6}	2.0×10^{-10}	5.9×10^{-10}
	432	nd	nd	3.78	4.75	7.85	-	-	-	-
	744	19.16	-1.61	3.64	4.82	7.91	1.1×10^{-6}	3.3×10^{-6}	3.1×10^{-11}	9.1×10^{-11}
	1056	24.07	1.37	3.29	4.79	8.01	1.3×10^{-6}	3.9×10^{-6}	2.6×10^{-11}	7.5×10^{-11}
	1440	23.85	1.35	3.57	5.01	7.97	1.3×10^{-6}	3.8×10^{-6}	1.9×10^{-11}	5.5×10^{-11}
	1752	28.35	4.14	3.40	4.80	7.99	1.5×10^{-6}	4.4×10^{-6}	1.8×10^{-11}	5.1×10^{-11}
	2112	39.89	11.63	3.25	4.67	8.06	1.9×10^{-6}	5.8×10^{-6}	1.9×10^{-11}	5.6×10^{-11}
	2448	34.85	8.35	3.24	4.58	8.00	1.8×10^{-6}	5.4×10^{-6}	1.5×10^{-11}	4.3×10^{-11}
	2784	45.93	15.27	3.08	4.77	8.02	2.2×10^{-6}	6.4×10^{-6}	1.6×10^{-11}	4.8×10^{-11}
3000	48.30	16.49	2.93	nd	8.03	2.3×10^{-6}	6.7×10^{-6}	1.6×10^{-11}	4.6×10^{-11}	
Average ^b								$1.98 \pm 0.57 \times 10^{-11}$	$5.83 \pm 1.65 \times 10^{-11}$	
control 1	1679	-	-	1.72	3.71	7.83	-	-	-	-

<i>control 2</i>	2112	-	-	2.44	4.26	7.78	-	-	-	-
<i>control 3</i>	3000	-	-	2.43	4.31	7.97	-	-	-	-

780 ^aDIC = dissolved inorganic carbon, determined with PHREEQC from measured fluid
781 composition. ^bAverage calculated for all time points after 72 h and less than 2112 h in the large
782 calcite experimental series and all time points after 72 h in the small and synthetic calcite
783 experimental series.

784
785
786

Figure Captions

787

788 **Figure 1.** X-ray diffraction patterns of initial calcite.

789

790 **Figure 2.** Scanning electron micrographs of initial large (a), small (b), and synthetic (c) calcite,
791 and calcite at the end of the experiments for the large from the second experimental series (d;
792 5926 h), small (e; 3000 h), and synthetic (f; 3000 h) calcite.

793

794 **Figure 3.** Fluid composition versus time. a) Calcium concentrations versus time, b) Dissolved
795 inorganic carbon concentrations versus time, c) pH versus time, and d) calcite saturation index
796 versus time.

797

798 **Figure 4.** Isotopic composition of calcite over time in a) large natural calcite experimental
799 series during the first 2112 h, b) small natural calcite experimental series, c) synthetic calcite
800 experiments, and d) large natural calcite experiments for the total time series. Error bars are
801 smaller than symbols employed if not otherwise visible.

802

803 **Figure 5.** Rate of isotope exchange versus time in all experiments. a) Carbon isotope exchange
804 rates. b) Oxygen isotope exchange rates.

805

806 **Figure 6.** Stoichiometry of C and O isotope exchange.

807

808 **Figure 7.** Modeled versus measured extent of ^{13}C exchanged with the fluid in a diffusion
809 controlled reaction for small natural calcite. Experimental data are represented by circles,
810 modelled data with dashed lines. Modelled lines are calculated using equation 6. The diffusion
811 coefficients used for model calculations are indicated on the plot and were estimated from the
812 experimental data either for the final data point ($D = 1.1 \times 10^{-23}$; this study 1) or for a visual best
813 fit of the data ($D = 4.0 \times 10^{-24}$; this study 2), and from Gehin et al. (2021) ($D = 1 \times 10^{-25}$) and
814 Lahav and Bolt (1964) (8.0×10^{-24}).

815

816

817 **Appendix A. Supplementary Material**

818

819 The supplementary material includes two files, one with two figures, and the other a
820 spreadsheet comprising raw XRD data. All other data are included in the manuscript.

821

822 **References**

823

824 Anderson, T.F., 1969. Self-diffusion of carbon and oxygen in calcite by isotope exchange with
825 carbon dioxide. *J. Geophys. Res.* 74, 3918–3932.

826 Arvidson, R.S., Luttge, A., 2010. Mineral dissolution kinetics as a function of distance from
827 equilibrium - New experimental results. *Chem. Geol.* 269, 79–88.

828 Avrahamov, N., Sivan, O., Yechieli, Y., Lazar, B., 2013. Carbon isotope exchange during calcite
829 interaction with brine: Implications for ¹⁴C dating of hypersaline groundwater.
830 *Radiocarbon* 55, 81–101.

831 Beard, B.L., Handler, R.M., Scherer, M.M., Wu, L., Czaja, A.D., Heimann, A., Johnson, C.M.,
832 2010. Iron isotope fractionation between aqueous ferrous iron and goethite. *Earth Planet.*
833 *Sci. Lett.* 295, 241–250.

834 Beard, B.L., Johnson, C.M., 2009. Atom Exchange between Aqueous Fe(II) and Goethite: An Fe
835 Isotope Tracer Study. *Environ. Sci. Technol.* 43, 1102–1107.

836 Bernard, S., Daval, D., Ackerer, P., Pont, S., Meibom, A., 2017. Burial-induced oxygen-isotope
837 re-equilibration of fossil foraminifera explains ocean paleotemperature paradoxes. *Nat.*
838 *Commun.* 8, 1–10.

839 Chanda, P., Gorski, C.A., Oakes, R.L., Fantle, M.S., 2019. Low temperature stable mineral
840 recrystallization of foraminiferal tests and implications for the fidelity of geochemical
841 proxies. *Earth Planet. Sci. Lett.* 506, 428–440.

842 Cherniak D. J. (2010) Diffusion in carbonates, fluorite, sulfide minerals, and diamond. *Rev.*
843 *Mineral. Geochemistry* **72**, 871–897.

844

845 Cisneros-Lazaro, D., Adams, A., Guo, J., Bernard, S., Baumgartner, L.P., Daval, D., Baronnet,
846 A., Grauby, O., Vennemann, T., Stolarski, J., Escrig, S., Meibom, A., 2022. Fast and pervasive
847 diagenetic isotope exchange in foraminifera tests is species-dependent. *Nat. Commun.* 13.
848 Coggon, R.M., Teagle, D.A.H., Smith-Duque, C.E., Alt, J.C., Cooper, M.J., 2010.
849 Reconstructing Past Seawater Mg/Ca. *Science* (80-.). 327, 1114–1117.
850 Cole, D.R., Chakraborty, S., 2001. Rates and mechanisms of isotopic exchange. *Rev. Mineral.*
851 *Geochemistry* 43, 83–223.
852 Crank, J., 1975. *The Mathematics Of Diffusion.* Oxford Univ. 50, 411.
853 Curti, E., Fujiwara, K., Iijima, K., Tits, J., Cuesta, C., Kitamura, A., Glaus, M.A., Müller, W.,
854 2010. Radium uptake during barite recrystallization at $23\pm 2^\circ\text{C}$ as a function of solution
855 composition: An experimental ^{133}Ba and ^{226}Ra tracer study. *Geochim. Cosmochim. Acta*
856 74, 3553–3570.
857 Daëron M., Drysdale R. N., Peral M., Huyghe D., Blamart D., Coplen T. B., Lartaud F. and
858 Zanchetta G. (2019) Most Earth-surface calcites precipitate out of isotopic equilibrium. *Nat.*
859 *Commun.* **10**, 1–7.
860
861 Dekens, P.S., Lea, D.W., Pak, D.K., Spero, H.J., 2002. Core top calibration of Mg/Ca in tropical
862 foraminifera: Refining paleotemperature estimation. *Geochemistry, Geophys. Geosystems*
863 3, 1–29.
864 Dubnina, E.O., Lakshatanov, L.Z., 1997. A kinetic model of isotopic exchange. *Geochimica* 61,
865 2265–2273.
866 Fantle, M.S., Tipper, E.T., 2014. Calcium isotopes in the global biogeochemical Ca cycle:
867 Implications for development of a Ca isotope proxy. *Earth-Science Rev.* 129, 148–177.

868 Fernandez, N.M., Zhang, X., Druhan, J.L., 2019. Silicon isotopic re-equilibration during
869 amorphous silica precipitation and implications for isotopic signatures in geochemical
870 proxies. *Geochim. Cosmochim. Acta* 262, 104–127.

871 Friedrich, O., Norris, R.D., Erbacher, J., 2012. Evolution of middle to late Cretaceous oceans-A
872 55 m.y. Record of Earth's temperature and carbon cycle. *Geology* 40, 107–110.

873 Frierdich, A.J., Beard, B.L., Reddy, T.R., Scherer, M.M., Johnson, C.M., 2014. Iron isotope
874 fractionation between aqueous Fe(II) and goethite revisited: New insights based on a multi-
875 direction approach to equilibrium and isotopic exchange rate modification. *Geochim.*
876 *Cosmochim. Acta* 139, 383–398.

877 Füger, A., Bruggmann, S., Frei, R., Leis, A., Dietzel, M., Mavromatis, V., 2019. The role of pH
878 on Cr(VI) partitioning and isotopic fractionation during its incorporation in calcite.
879 *Geochim. Cosmochim. Acta* 265, 520–532.

880 Garnier, J.M., 1985. Retardation of dissolved radiocarbon through a carbonated matrix.
881 *Geochim. Cosmochim. Acta* 49, 683–693.

882 Géhin, A., Gilbert, B., Chakraborty, S., Stack, A.G., Allard, L.F., Robinet, J.C., Charlet, L.,
883 2021. Long-Term ^{13}C Uptake by ^{12}C -Enriched Calcite. *ACS Earth Sp. Chem.* 5, 998–1005.

884 Gorski, C.A., Fantle, M.S., 2017. Stable mineral recrystallization in low temperature aqueous
885 systems: A critical review. *Geochim. Cosmochim. Acta* 198, 439–465.

886 Grimm, C., Mavromatis, V., Leis, A., Pokrovsky, O.S., Oelkers, E.H., 2021. The temporal
887 evolution of the carbon isotope composition of calcite in the presence of cyanobacteria.
888 *Chem. Geol.* 584, 120556.

889 Gussone, N., Schmitt, A.-D., Heuser, A., Wombacher, F., Dietzel, M., Tipper, E., Schiller, M.,
890 2016. *Advances in isotope geochemistry - Calcium stable isotope geochemistry*. Springer-

891 Verlag.

892 Haul, R.A.W., Stein, L.H., 1955. Diffusion in calcite crystals on the basis of isotopic exchange
893 with carbon dioxide. *Trans. Faraday Soc.* 51, 1280–1290.

894 Hellmann, R., Tisserand, D., 2006. Dissolution kinetics as a function of the Gibbs free energy of
895 reaction: An experimental study based on albite feldspar. *Geochim. Cosmochim. Acta* 70,
896 364–383.

897 Hoefs, J., 1997. Stable isotope geochemistry, *Earth-Science Reviews*.

898 Katz, M.E., Cramer, B.S., Franzese, A., Hönisch, B., Miller, K.G., Rosenthal, Y., Wright, J.D.,
899 2010. Traditional and emerging geochemical proxies in foraminifera. *J. Foraminifer. Res.*
900 40, 165–192.

901 Kronenberg, A.K., Yund, R.A., Giletti, B.J., 1984. Carbon and oxygen diffusion in calcite:
902 Effects of Mn content and $p\text{H}_2\text{O}$. *Phys. Chem. Miner.* 11, 101–112.

903 Labotka, T.C., Cole, D.R., Fayek, M.J., Chacko, T., 2011. An experimental study of the diffusion
904 of C and O in calcite in mixed $\text{CO}_2\text{-H}_2\text{O}$ fluid. *Am. Mineral.* 96, 1262–1269.

905 Lahav, N., Bolt, G.H., 1964. Self-diffusion of Ca^{45} into certain carbonates. *Soil Sci.* 97, 293–
906 299.

907 Marriott, C.S., Henderson, G.M., Belshaw, N.S., Tudhope, A.W., 2004. Temperature
908 dependence of $\delta^7\text{Li}$, $\delta^{44}\text{Ca}$ and Li/Ca during growth of calcium carbonate. *Earth Planet.*
909 *Sci. Lett.* 222, 615–624.

910 Mavromatis, V., Gautier, Q., Bosc, O., Schott, J., 2013. Kinetics of Mg partition and Mg stable
911 isotope fractionation during its incorporation in calcite. *Geochim. Cosmochim. Acta* 114,
912 188–203.

913 Mavromatis, V., González, A.G., Dietzel, M., Schott, J., 2019. Zinc isotope fractionation during

914 the inorganic precipitation of calcite – Towards a new pH proxy. *Geochim. Cosmochim.*
915 *Acta* 244, 99–112.

916 Mavromatis, V., Montouillout, V., Noireaux, J., Gaillardet, J., Schott, J., 2015. Characterization
917 of boron incorporation and speciation in calcite and aragonite from co-precipitation
918 experiments under controlled pH, temperature and precipitation rate. *Geochim. Cosmochim.*
919 *Acta* 150, 299–313.

920 Mavromatis, V., van Zuilen, K., Purgstaller, B., Baldermann, A., Nägler, T.F., Dietzel, M., 2016.
921 Barium isotope fractionation during witherite (BaCO_3) dissolution, precipitation and at
922 equilibrium. *Geochim. Cosmochim. Acta* 190, 72–84.

923 Mayer, K.U., Frind, E.O., Blowes, D.W., 2002. Multicomponent reactive transport modeling in
924 variably saturated porous media using a generalized formulation for kinetically controlled
925 reactions. *Water Resour. Res.* 38, 13-1-13–21.

926 Mozeto, A.A., Fritz, P., Reardon, E.J., 1984. Experimental observations on carbon isotope
927 exchange in carbonate-water systems. *Geochim. Cosmochim. Acta* 48, 495–504.

928 Oelkers, E.H., Berninger, U.N., Pérez-Fernández, A., Chmeleff, J., Mavromatis, V., 2018. The
929 temporal evolution of magnesium isotope fractionation during hydromagnesite dissolution,
930 precipitation, and at equilibrium. *Geochim. Cosmochim. Acta* 226, 36–49.

931 Oelkers, E.H., Pogge von Strandmann, P.A.E., Mavromatis, V., 2019. The rapid resetting of the
932 Ca isotopic signatures of calcite at ambient temperature during its congruent dissolution,
933 precipitation, and at equilibrium. *Chem. Geol.* 512, 1–10.

934 Pearce, C.R., Saldi, G.D., Schott, J., Oelkers, E.H., 2012. Isotopic fractionation during congruent
935 dissolution, precipitation and at equilibrium: Evidence from Mg isotopes. *Geochim.*
936 *Cosmochim. Acta* 92, 170–183.

937 Pokrovsky, O.S., Mielczarski, J.A., Barres, O., Schott, J., 2000. Surface speciation models of
938 calcite and dolomite/ aqueous solution interfaces and their spectroscopic evaluation.
939 *Langmuir* 16, 2677–2688.

940 Ravelo, A.C., Hillaire-Marcel, C., 2007. The use of oxygen and carbon isotopes of foraminifera
941 in paleoceanography. Chapter 18, *Developments in Marine Geology* 1, 735–764.

942 Riechelmann, S., Mavromatis, V., Buhl, D., Dietzel, M., Hoffmann, R., Jöns, N., Kell-
943 Duivesteyn, I., Immenhauser, A., 2018. Echinoid skeletal carbonate as archive of past
944 seawater magnesium isotope signatures – Potential and limitations. *Geochim. Cosmochim.*
945 *Acta* 235, 333–359.

946 Schott, J., Brantley, S., Crerar, D., Guy, C., Borcsik, M., Willaime, C., 1989. Dissolution kinetics
947 of strained calcite. *Geochim. Cosmochim. Acta* 53, 373–382.

948 Schott, J., Oelkers, E.H., Benezeth, P., Godderis, Y., Francois, L., 2012. Can accurate kinetic
949 laws be created to describe chemical weathering? *Comptes Rendus Geosci.* 344, 568–585.

950 Sexton, P.F., Wilson, P.A., Pearson, P.N., 2006. Microstructural and geochemical perspectives
951 on planktic foraminiferal preservation: “glassy” versus “frosty.” *Geochemistry, Geophys.*
952 *Geosystems* 7.

953 Spero, H.J., Bijma, J., Lea, D.W., Bemis, B.E., 1997. Spero et al. 1997_N 497–500.

954 Stamm, F.M., Zambardi, T., Chmeleff, J., Schott, J., von Blanckenburg, F., Oelkers, E.H., 2019.
955 The experimental determination of equilibrium Si isotope fractionation factors among H_4
956 SiO_4^\ominus , H_3SiO_4^- and amorphous silica ($\text{SiO}_2 \cdot 0.32\text{H}_2\text{O}$) at 25 and 75°C using the three-
957 isotope method. *Geochim. Cosmochim. Acta* 255, 49–68.

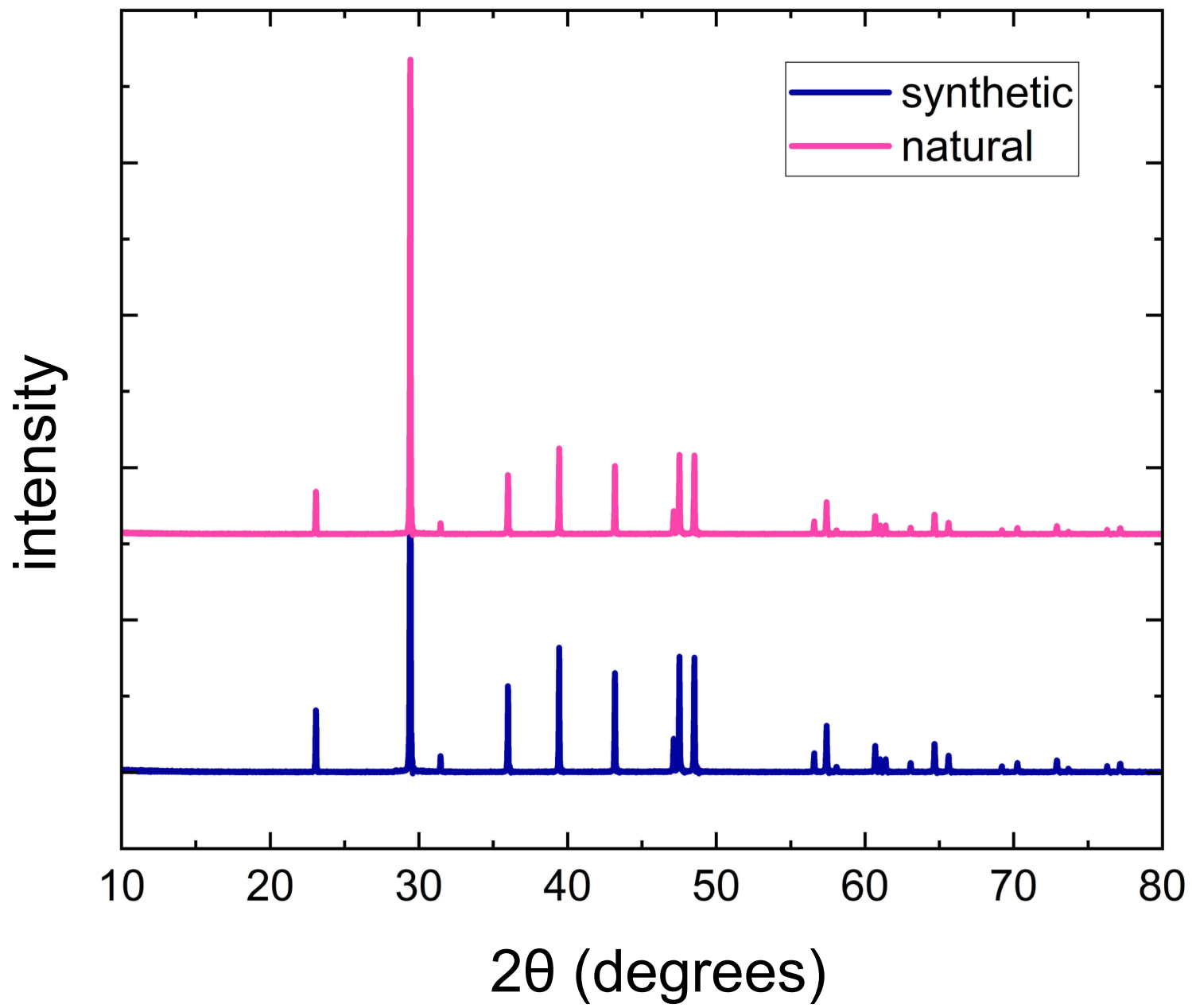
958 Subhas, A. V., Adkins, J.F., Rollins, N.E., Naviaux, J., Erez, J., Berelson, W.M., 2017. Catalysis
959 and chemical mechanisms of calcite dissolution in seawater. *Proc. Natl. Acad. Sci.* 114,

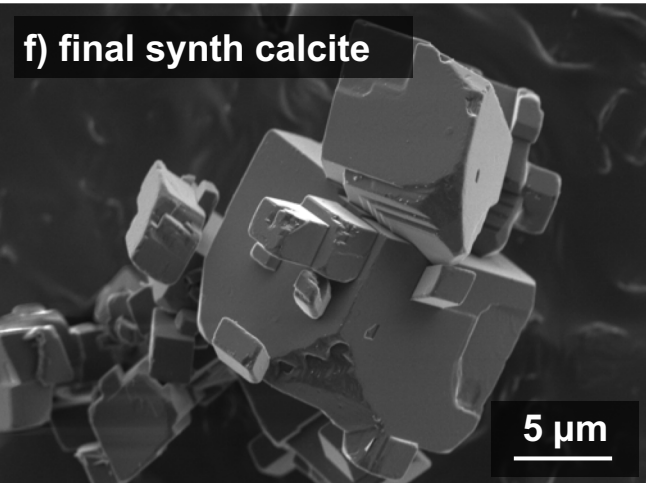
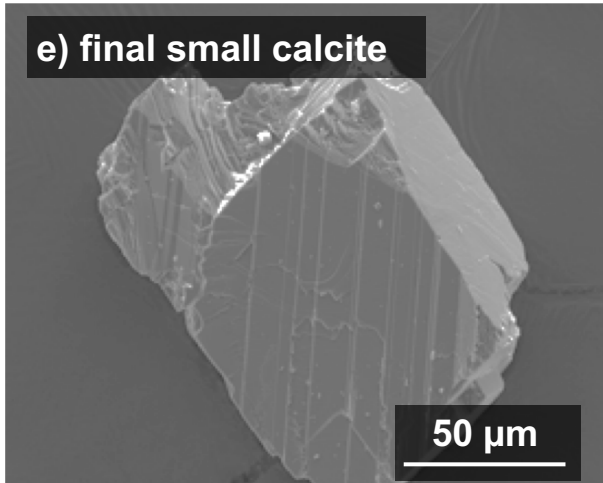
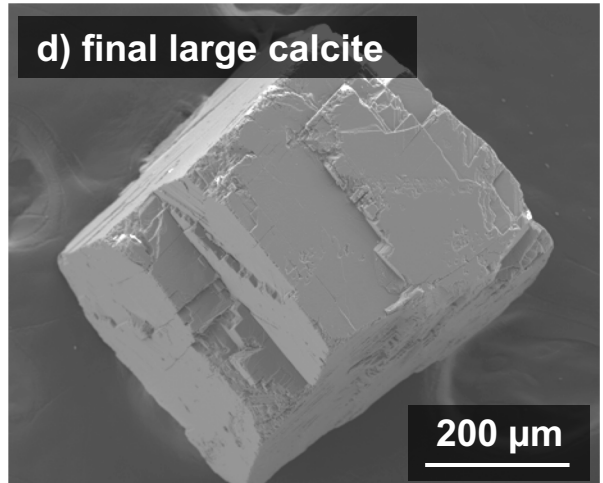
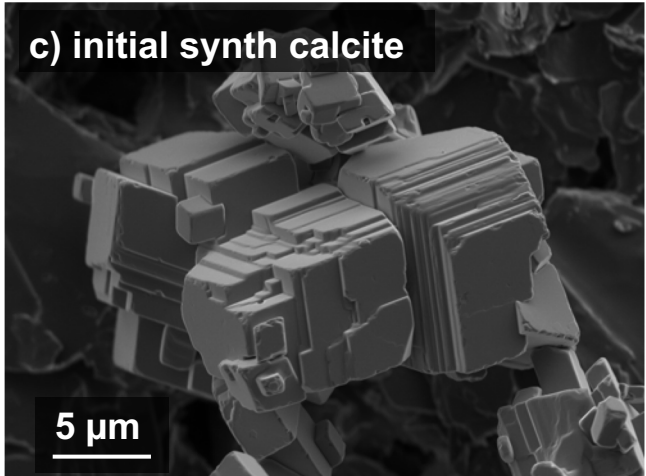
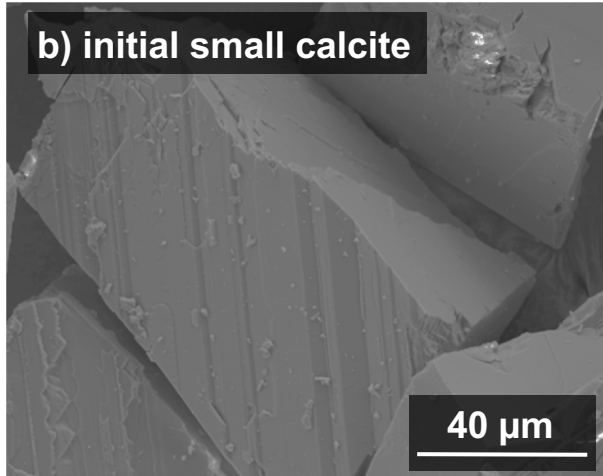
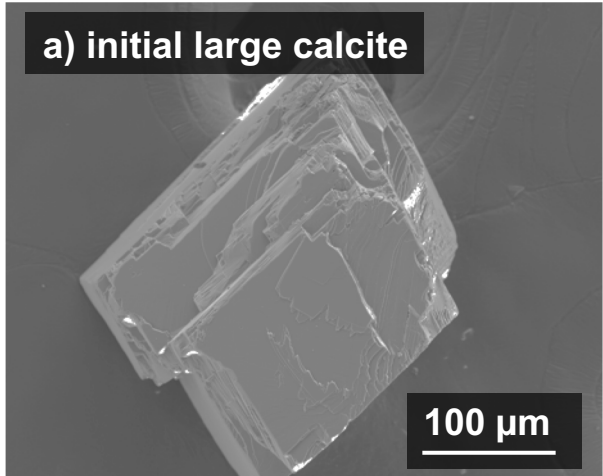
960 8175–8180.

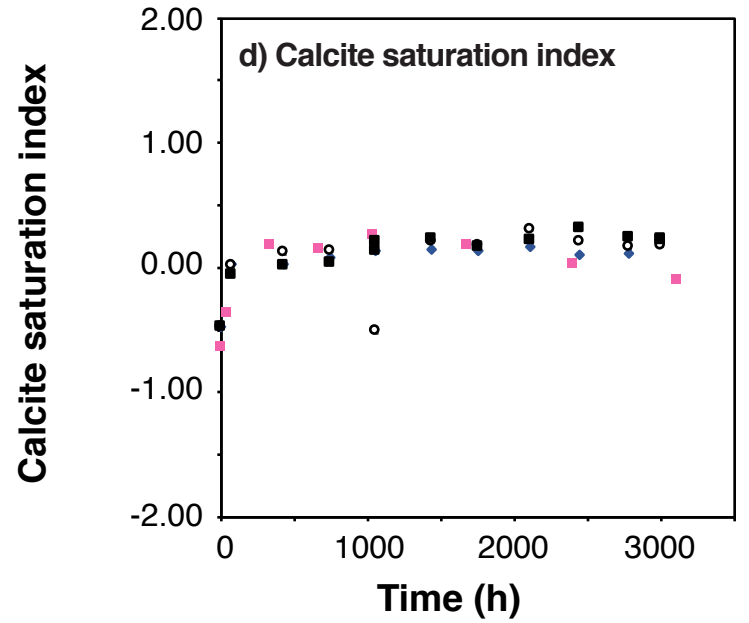
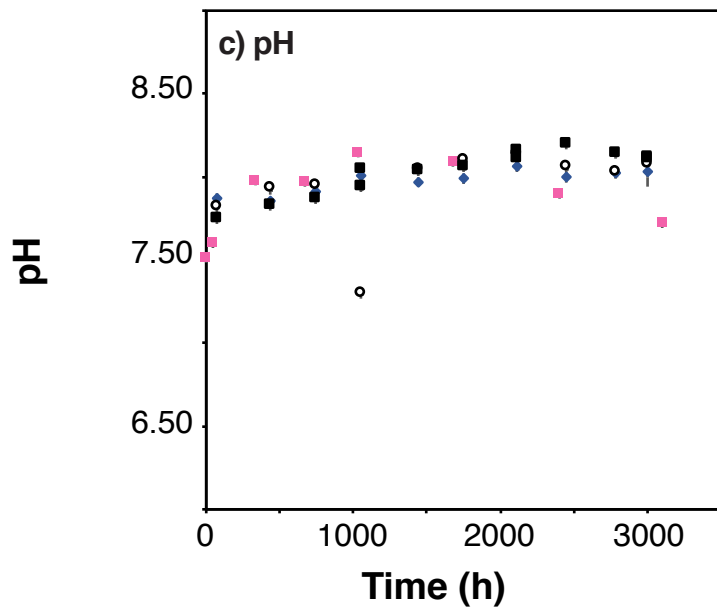
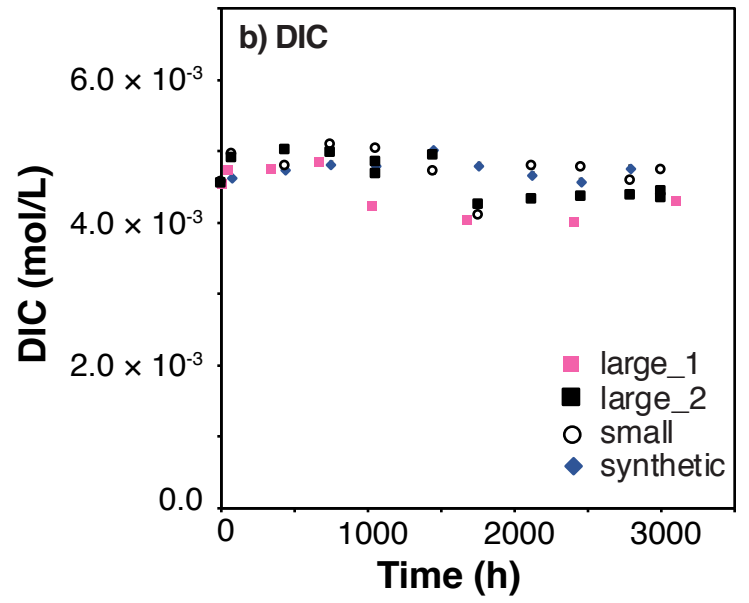
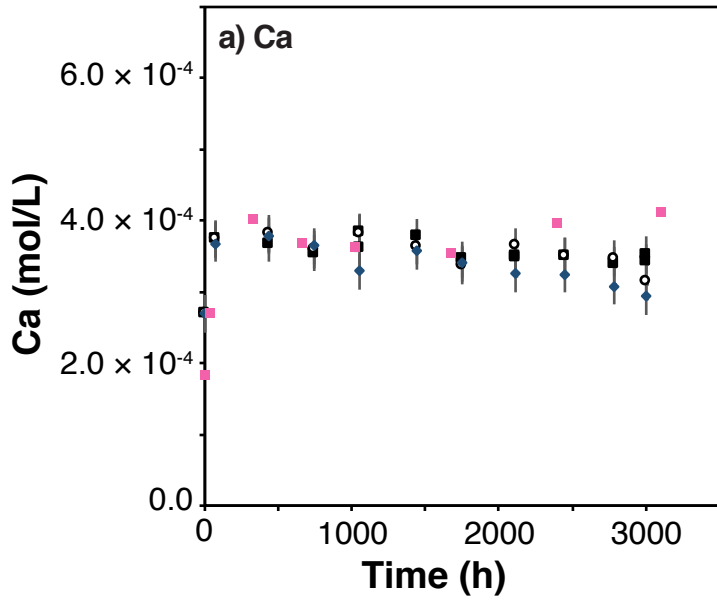
961 Urey, H.C., Lowenstam, H. a., Epstein, S., McKinney, C.R., 1951. Measurement of
962 paleotemperatures and temperatures of the upper cretaceous of England, Denmark, and the
963 Southeastern United States. *Bull. Geol. Soc. Am.* 62, 399–416.

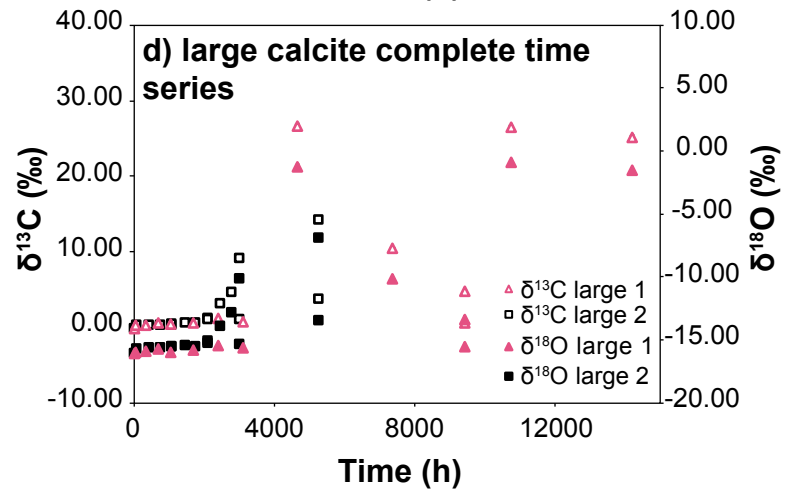
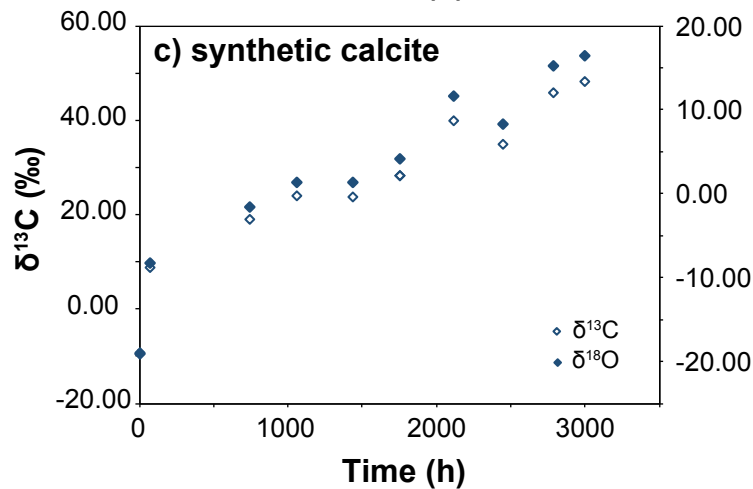
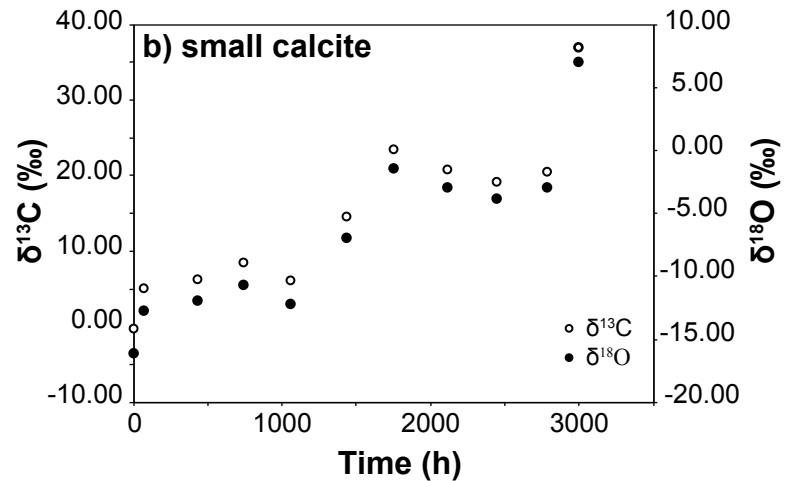
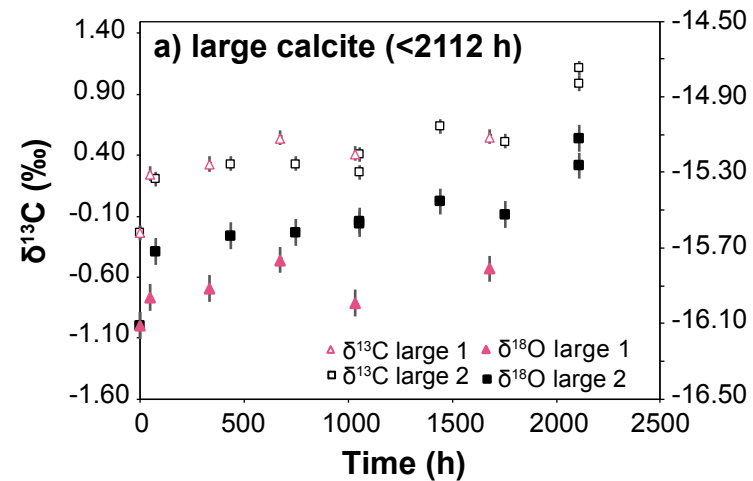
964 Zhu, C., Liu, Z., Zhang, Y., Wang, C., Scheafer, A., Lu, P., Zhang, G., Georg, R.B., Yuan, H.
965 lin, Rimstidt, J.D., 2016. Measuring silicate mineral dissolution rates using Si isotope
966 doping. *Chem. Geol.* 445, 146–163.

967

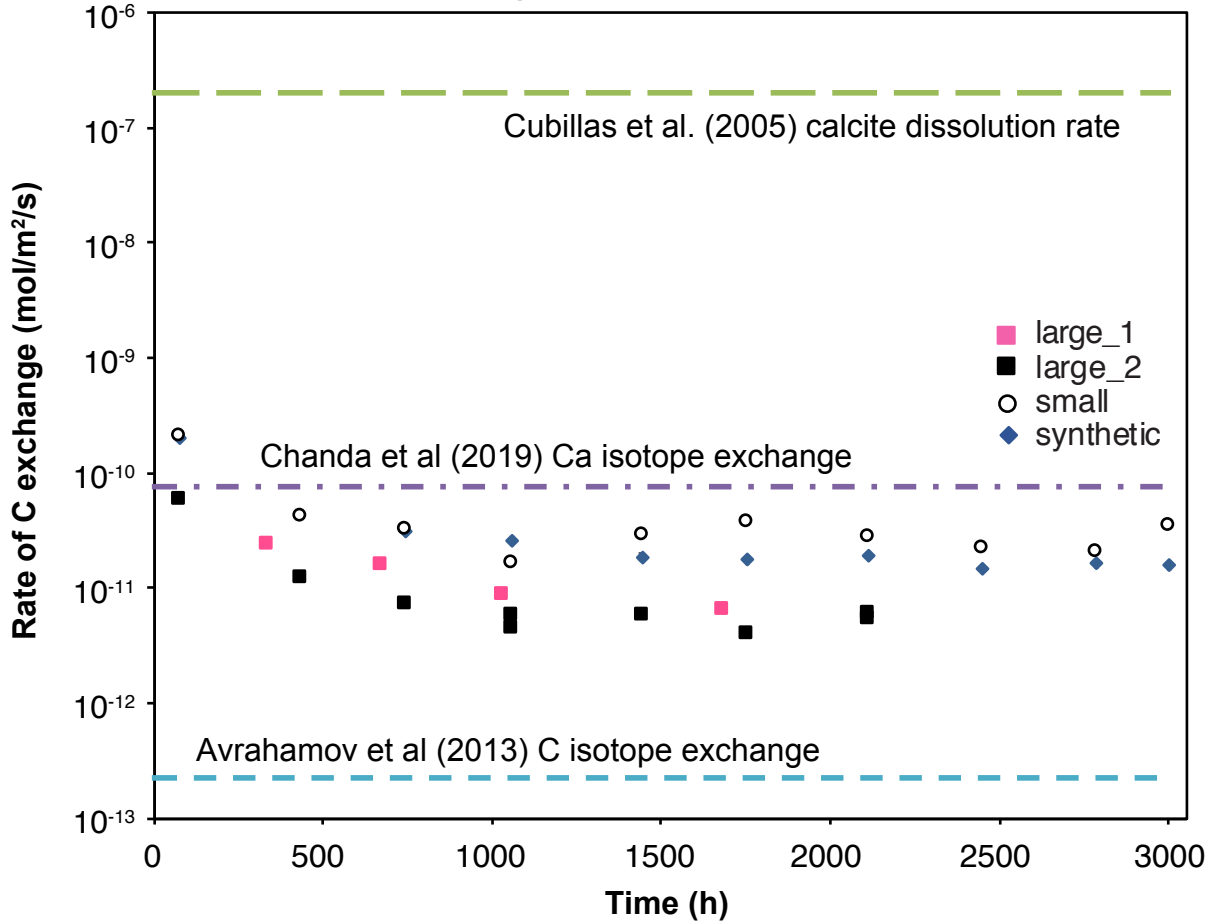








a) C isotope exchange rate



b) O isotope exchange rate

